Journal of Experimental Zoology Part B: Molecular and Developmental Evolution

WILEY

JEZ-B MOLECULAR AND DEVELOPMENTAL EVOLUTION

RESEARCH ARTICLE OPEN ACCESS

From Egg to Adult: A Developmental Table of the Ant *Monomorium pharaonis*

Arjuna Rajakumar[1,2] | Luigi Pontieri[3] | Ruyan Li[3] | Rasmus Stenbak Larsen[3] | Angelly Vásquez-Correa[1] | Johanne K. L. Frandsen[3] | Ab Matteen Rafiqi[4] | Guojie Zhang[3,5,6] | Ehab Abouheif[1]

[1]Department of Biology, McGill University, Montreal, Quebec, Canada | [2]Whitehead Institute for Biomedical Research, Cambridge, Massachusetts, USA | [3]Section for Ecology and Evolution, Department of Biology, University of Copenhagen, Copenhagen, Denmark | [4]Beykoz Institute of Life Science and Biotechnology, Bezmialem Vakif University, Beykoz, Istanbul, Turkey | [5]State Key Laboratory of Genetic Resources and Evolution, Kunming Institute of Zoology, Chinese Academy of Sciences, Kunming, Yunnan, China | [6]Centre for Evolutionary and Organismal Biology, and Women's Hospital, School of Medicine, Zhejiang University, Hangzhou, Zhejiang, China

Correspondence: Guojie Zhang (guojiezhang@zju.edu.cn) | Ehab Abouheif (ehab.abouheif@mcill.ca)

Received: 21 October 2020 | **Accepted:** 8 October 2024

Funding: This research was supported by a National Science Foundation EDGE grant (Award No. 2128304) to A.R., a Lundbeck Foundation Grant (R190-2014-2827) to G.Z., and an NSERC Discovery Grant (Canada) to E.A.

Keywords: ants | caste determination | caste differentiation | developmental table | embryonic development | germ cell | larval development | *Monomorium pharaonis* | polyphenism | pupal development

ABSTRACT

Ants are one of the most ecologically and evolutionarily successful groups of animals and exhibit a remarkable degree of phenotypic diversity. This success is largely attributed to the fact that all ants are eusocial and live in colonies with a reproductive division of labor between morphologically distinct queen and worker castes. Yet, despite over a century of studies on caste determination and evolution in ants, we lack a complete ontogenetic series from egg to adult for any ant species. We, therefore, present a developmental table for the Pharaoh ant *Monomorium pharaonis*, a species whose colonies simultaneously produce reproductive queens and completely sterile workers. In total, *M. pharaonis* embryonic, larval, and pupal development lasts 45 days. During embryogenesis, the majority of developmental events are conserved between *M. pharaonis* and the fruit fly *Drosophila melanogaster*. We discovered, however, two types of same-stage embryos before gastrulation: (1) embryos with internalized germ cells; and (2) embryos with germ cells outside of the blastoderm at the posterior pole. Moreover, we also found two-types of embryos following germ band extension: (1) embryos with primordial germ cells that will develop into reproductive queens; and (2) embryos with no germ cells that will develop into completely sterile workers. Together, these data show that queen and worker castes are already determined and differentiated by early embryogenesis. During larval development, we confirmed that reproductive and worker larvae proceed through three larval instars. Using anatomical and developmental markers, we can further discern the development of gyne (unmated queen) larvae, male larvae, and worker larvae as early as the 1st instar. Overall, we hope that the ontogenetic series we present here will serve as a blueprint for the generation of future ant developmental tables.

1 | Introduction

A major goal of evolutionary developmental biology (evo–devo) is to understand how developmental systems evolve and influence the evolution of genotypes and phenotypes (Arthur 2002; Hall and Olson 2006; Carroll 2008; Hall 2012; Wagner 2014; Love 2014; Moczek et al. 2015). Over the last four decades, evo–devo has shown that the diversity in animal body

Arjuna Rajakumar and Luigi Pontieri contributed equally to this article.

plans involves tinkering with a relatively small number of highly conserved developmental regulatory genes, known as the "genetic toolkit" (Patel 1994; Quiring et al. 1994; Carroll 1995; Gerhart and Kirschner 1997; Akam 1998; Hall 2003; Carroll 2005; Davidson and Erwin 2006; Peter and Davidson 2016; Hu, Linz, and Moczek 2019; Bruce and Patel 2020; Murugesan et al. 2022). Evo–devo studies on ants have played a crucial role in revealing the ecological dimensions of *evo–devo*, a re-emerging synthesis known as *eco–evo–devo* (Metzl, Wheeler, and Abouheif 2018). This field explores how the interaction between this highly conserved genetic toolkit and environmental factors, such as nutrition, temperature, and social interactions, can influence phenotypic variation and evolutionary change (Evans and Wheeler 1999; Miura et al. 1999; West-Eberhard 2003; Abouheif et al. 2014; Gilbert, Bosch, and Ledón-Rettig 2015; Emilia Santos et al. 2015; Sommer and Mayer 2015; Toth and Rehan 2017; Sanger and Rajakumar 2018; Kapheim et al. 2020).

Ants are particularly exciting models for *eco–evo–devo* because all ants are obligately eusocial, meaning that individuals live in colonies and have a reproductive division of labor with overlapping adult generations and cooperative brood care (Crespi and Yanega 1995). Individuals within a colony have also evolved different phenotypes called "castes," where they belong either to the reproductive caste (gynes/queens or males) or to the worker caste. Caste determination occurs during development and is polyphenic, such that eggs laid by the queen can initiate the queen or worker developmental program in response to environmental cues (Brian 1974; Passera and Suzzoni 1979; Hölldobler and Wilson 1990; Hölldobler and Wilson 2009; Penick, Prager, and Liebig 2012). In most ant species, queen and worker castes display dramatic differences in morphology and life history. Key differences include wing polyphenism, where colonies develop winged queens and wingless workers; a size and reproductive asymmetry between a large hyperfertile queen caste and small subfertile worker caste; and within the worker caste, the evolution of a novel soldier subcaste. Each of these innovations evolved through the differential regulation of the genetic toolkit during either embryonic, larval, or pupal stages (Abouheif and Wray 2002; Wheeler and Nijhout 2003; Sameshima, Miura, and Matsumoto 2004; Gotoh et al. 2005, 2016; Khila and Abouheif 2008, 2010; Rajakumar et al. 2012, 2018; Béhague et al. 2018; Oettler et al. 2019; Yan et al. 2022; Brahma et al. 2023). Furthermore, within ant societies, developing larvae play fundamental roles in social regulation, such as in processing food, producing pheromones, and regulating caste-ratio, further increasing the complex regulatory landscape of colonial life (Mamsch 1967; Villalta et al. 2015; Ebie, Hölldobler, and Liebig 2015; Warner, Kovaka, and Linksvayer 2016; Schultner, Oettler, and Helanterä 2017; Warner et al. 2019; Snir et al. 2022).

To date, empirical eco–evo–devo studies on ants have helped us to understand: queen–worker caste differentiation (Passera and Suzzoni 1979; Wheeler 1986; Abouheif and Wray 2002; Sameshima, Miura, and Matsumoto 2004; Gotoh et al. 2005; Khila and Abouheif 2008, 2010; Miyazaki et al. 2010; Penick, Prager, and Liebig 2012; Qui et al. 2018; Chandra et al. 2018; Warner et al. 2019; Nagel et al. 2020; Qiu et al. 2022; Yan et al. 2022; Trible et al. 2023); epigenetic regulation (Alvarado et al. 2015; LeBoeuf et al. 2016; Simola et al. 2016; Glastad, Ju, and Berger 2021; Gospocic et al. 2021); worker polymorphism (Passera 1974; Wheeler and Nijhout 1981a; 1981b; Rajakumar et al. 2018; Klein et al. 2016); social behavior (Teseo et al. 2014; Trible et al. 2017; Yan et al. 2017; Glastad, Ju, and Berger 2021; Gospocic et al. 2021; Brahma et al. 2023; Ju et al. 2023); modularity (Yang and Abouheif 2011; Londe et al. 2015; Hart et al. 2024); evolutionary novelty (Rajakumar et al. 2012, 2018; Favé et al. 2015; Powell, Price, and Kronauer 2020; Rafiqi, Rajakumar, and Abouheif 2020); gene by environment interactions (Schrader et al. 2014, 2021; Singh and Linksvayer 2020; Glastad et al. 2023); ancestral developmental potentials (Rajakumar et al. 2012); and major evolutionary transitions in individuality (Bernadou et al. 2018; Rafiqi, Rajakumar, and Abouheif 2020). Despite the success of these eco–evo–devo studies in ants, there is a general absence of a detailed ontogenetic series from egg to adult for any ant species. This has hampered our ability to advance the functional characterization of the genes and gene networks underlying key innovations in ants, such as those regulating caste determination between queens and workers. For example, the ability to establish transgenic lines with CRISPR-CAS9 gene editing in any organism is predicated on a working knowledge of the timing and stages of that organism's development. This is evident in recent studies that have functionally manipulated gene expression during development in different ant lineages, where an understanding of developmental timing was required to ensure the specificity and efficacy of reagents to downregulate gene expression (Alvarado et al. 2015; Trible et al. 2017; Yan et al. 2017, 2022; Rajakumar et al. 2018; Rafiqi, Rajakumar, and Abouheif 2020; Gospocic et al. 2021; Qiu et al. 2022; Glastadet al. 2023; Ju et al. 2023; Hart et al. 2023).

The general lack of developmental tables in ants is surprising given the long and rich history of the study of ant development. Before the rise of inclusive fitness theory (Hamilton 1964a, 1964b), a group of biologists generated a body of pioneering work on the eco–evo–devo of ants (Metzl, Wheeler, and Abouheif 2018). This pioneering work includes studies by Wheeler (1893, 1910, 1911), Goestch (1937, 1939), Bier (1952), and Dewitz (1878), all of whom made prescient insights into the developmental basis of caste determination. Furthermore, work by Ganin (1869), Tanquary (1912), Blochmann (1892), Strindberg (1913, 1915a, 1915b, 1916, 1917), Hegner (1915), Lilienstern (1932), and Buchner (1918, 1965) began investigating, in remarkable detail, ant embryogenesis (Figure 1). To our knowledge, Ganin (1869) is one of the first to present an ontogenetic series of ant embryonic development, in which he described the embryonic development of *Formica fusca*, from the syncytial blastoderm stage through to segmentation. Later, Wheeler (1918, 1922) described the general morphology of ant larvae, and in 1947, Athias-Henriot (1947) provided the first detailed account of the internal anatomy of larvae. Finally, George Wheeler and Jeanette Wheeler, who in a long series of publications between 1953 and 1990 extensively described the external morphology of larvae of approximately 800 species of ants (Wheeler and Wheeler 1953, 1955,

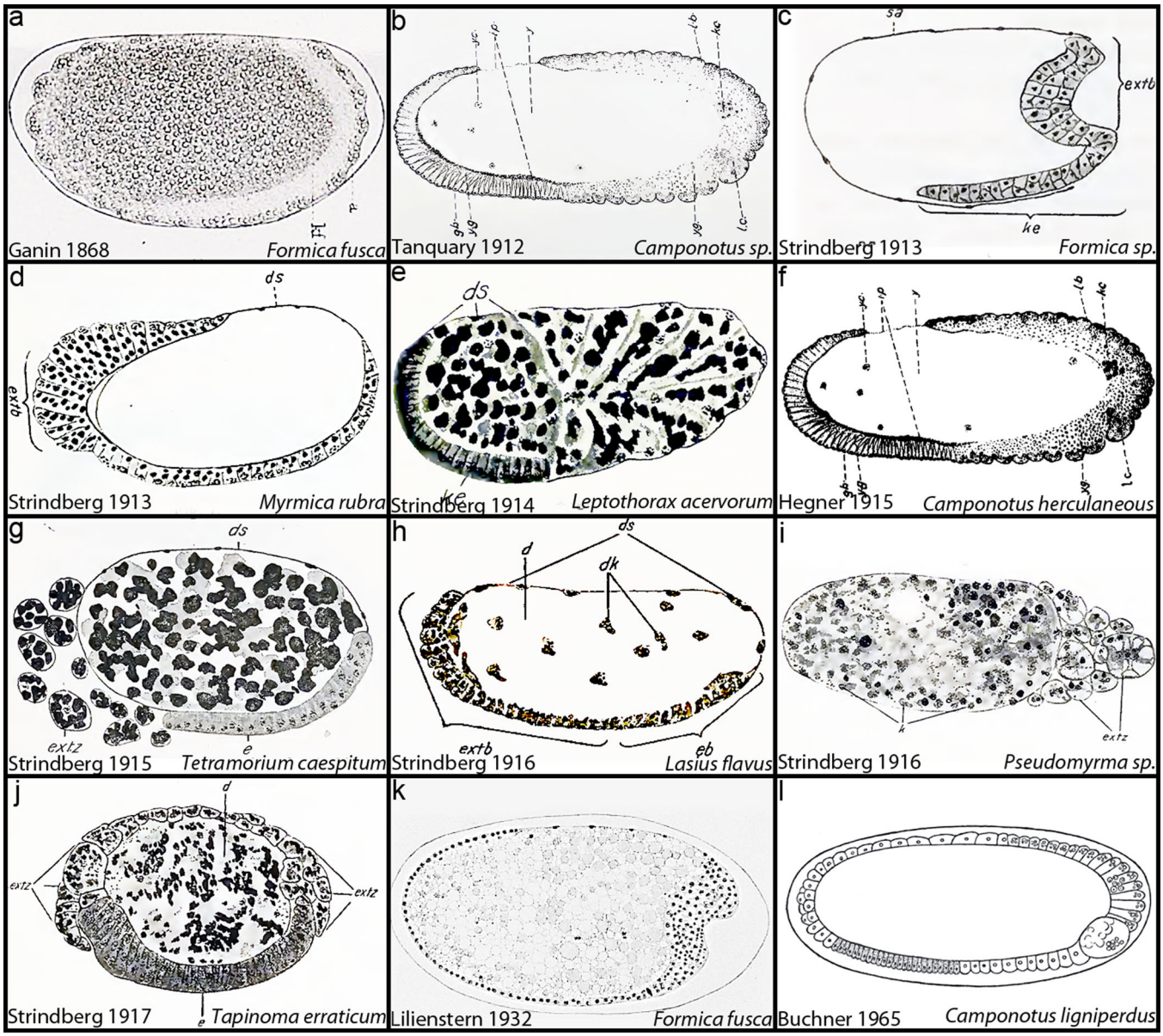

FIGURE 1 | A century of ant embryology. (a–l) Histological sections of cellular blastoderm or gastrulation stage embryos representing four ant subfamilies adapted from historical references. Embryos are in chronological order of their description. (a) *Formica fusca* embryo adapted from Ganin (1869). (b) *Camponotus sp*. embryo adapted from Tanquary (1912). (c) *Formica sp*. embryo adapted from Strindberg (1913). (d) *Myrmica rubra* embryo adapted from Strindberg (1913). (e) *Leptothorax acervorum* embryo adapted from Strindberg (1915a). (f) *Camponotus herculaneous* embryo adapted from Hegner (1915). (g) *Tetramorium caespitum* embryo adapted from Strindberg (1915b). (h) *Lasius flavus* embryo adapted from Strindberg (1916). (i) *Pseudomyrma sp*. embryo from Strindberg (1916). (j) *Tapinoma erraticum* embryo adapted from Strindberg (1917). (k) *F. fusca* embryo adapted from Lilienstern (1932). (l) *Camponotus ligniperdus* adapted from Buchner (1965). Anterior is to the left, posterior to the right, dorsal up, ventral down, except panels (e) and (h) where posterior is to the left and anterior to the right.

1976, 1990). Only more recently have researchers begun to describe in detail the number of instars of a given ant species (Passera and Vllème 1973; O'Neal and Markin 1975; Petralia and Vinson 1979; Wheeler 1982; Sameshima, Miura, and Matsumoto 2004; Fox et al. 2012, 2017; Masuko 2017; Solis et al. 2010; Alvarado et al. 2015; Koch et al. 2021).

We therefore characterized an ontogenetic series, spanning embryonic, larval, and pupal stages of the Pharaoh ant *Monomorium pharaonis*, a global invasive species (Pontieri and Linksvayer 2021). *M. pharaonis* colonies are polygynous (multiple queens), monoandrous (singly mated), and have a monomorphic worker caste (limited size variation) (Jackson, Holcombe, and Ratnieks 2004). Over the last decade, *M. pharaonis* has been used as a model to study the socio-genomic basis of social insect castes (Pontieri et al. 2017; Qui et al. 2018; Walsh et al. 2018; Warner et al. 2019; Walsh, Garnier, and Linksvayer 2020; Singh and Linksvayer 2020; Nagel et al. 2020; Li et al. 2022; Qiu et al. 2022), collective behaviors (Gordon 2019; Walsh et al. 2020; Walsh, Garnier, and Linksvayer 2020), and caste/sex ratio regulation (Warner, Kovaka, and Linksvayer 2016; Pontieri et al. 2017; Warner, Lipponen, and Linksvayer 2018; Singh and Linksvayer 2020). *M. pharaonis* is also a promising model for

studying gene–environment interactions during development and evolution because reproductive gynes (unmated queens) and males practice within nest mating, whereas workers are obligately sterile and lack a germline. As such, only queens can produce brood within a colony (Hölldobler and Wilson 1990). These features make it possible to establish and maintain colony lineages, or "sociogenetic lines," for several generations in the lab (Walsh, Garnier, and Linksvayer 2020). Furthermore, reproductives can be mated with unrelated partners, allowing the establishment of genetically heterogeneous crossed lines (Schmidt et al. 2011; Pontieri et al. 2017). Finally, *M. pharaonis* is particularly suited for addressing the question of caste determination and differentiation. Unlike the majority of ant species where queens produce gynes and males during only a short period of the year, *M. pharaonis* produces all castes and sexes year-round, thereby enabling the ability to study the developmental programs of all castes at the same time (i.e., worker, gyne, male) (Edwards 1987; Qiu et al. 2022). Our general aim is that a developmental table of *M. pharaonis* will facilitate all these areas of study, especially the eco–evo–devo of ants.

2 | Materials and Methods

2.1 | Ant Colony Maintenance and Collection of Eggs, Larvae, and Prepupae

Two colonies (D03 and 4030) of *M. pharaonis* were used in this study to collect egg, larval, prepupal, and pupal stages. This colony was part of a larger stock of colonies artificially created in 2010 through the sequential cross of eight inbred lineages (see Schmidt et al. 2011 and Pontieri et al. 2017 for breeding methods) and has since been maintained at the University of Copenhagen. The colonies were kept at 27°C ± 1°C and 50% RH in a plastic box (27 × 17 × 9.5 cm) coated with Fluon (polytetrafluorethylene, De Monchy, The Netherlands), with cotton-sealed plastic tubes serving as nesting sites. The colony was fed twice a week with a standardized diet containing a 1:4 ratio of total proteins to digestible carbohydrates (diet modified from Dussutour and Simpson 2008) and house crickets (*Acheta domesticus*, QB Insects, Linnich, Germany). Water was provided ad libitum.

For timed egg collections, 15 queens were removed from the colony using a fine brush and placed in a Fluon-coated petri dish (15 cm × 1.5 cm) containing a 2 cm^2 piece of black cardboard to nest underneath. Queens were provided with 80 workers from their colony, a piece of food and a water tube. Queens were left to lay eggs for different intervals to determine how long a given embryonic stage lasts. Egg depositions were either collected at the same time as queen removal (for Stages 1 and 2) or aged in the petri dish (for Stages 3 and onwards), with workers tending them. Food was replaced daily, and petri dishes containing aging eggs were kept at the same temperature and humidity condition as the stock colony. Eggs were then collected at the desired stage and fixed.

Larval stages used for morphometric analyses were collected from two sub-colonies established by splitting in half the colony used for egg depositions. Previous studies have shown that the removal of queens allows workers to raise existing reproductive brood to adulthood (Edwards 1987). Therefore, two sub-colonies were created to facilitate the collection of worker-destined and reproductive-destined brood. The first sub-colony, containing approximately 50 queens, was used to collect 1st larval instars of unknown caste, 2nd and 3rd worker larval instars. The second sub-colony, dequeened at the time of its establishment to trigger the production of new reproductives (gynes and males), was used to collect 1st larval instars of unknown caste, 2nd and 3rd reproductive larval instars. Individual larvae and prepupae were collected using a fine brush and gently lined up, with the cephalic capsule facing up, on a piece of double-side tape which was then placed on a microscope slide for imaging.

2.2 | Embryo Fixation and Nuclear Staining

Embryos were gently transferred with a moistened brush in an incubation basket with a 100 μm mesh (Intavis Bioanalytical Instruments AG), dechorionated in 25% commercial bleach (from a 12.5% sodium hypochlorite stock) for 2 min and quickly washed under demineralized tap water for 30 s. Embryos were then bathed in 0.3% PBTx (1× PBS, Triton X-100 – Sigma Aldrich) for 5 min on ice, heat fixed by boiling for 30 s in 0.3% PBTx, quickly quenched in 1× PBS on ice and finally bathed in 0.1% PBTw (1× PBS, Tween-20 – Sigma Aldrich) on ice for 5 min. Embryos were then washed four times in PBTw (5 min each wash), fixed in 4% paraformaldehyde for 30 min at room temperature, and then washed once with 1× PBS. Fixed embryos were transferred from the incubation basket to a 2 mL screw top clear glass vial (Supelco; Sigma-Aldrich) using a glass Pasteur pipette. After removing the 1× PBS, 500 μL of ice-cold methanol was added and the vial was vigorously shaken for 10 s. Embryos were finally washed two times with ice cold methanol and either stored at −20°C or immediately rehydrated. While in other insects this methanol shock helps to crack the vitelline membrane or remove it entirely (Rafiqi, Lemke, and Schmidt-Ott 2011), in *M. pharaonis* we found ice cold methanol did not remove the vitelline membrane but instead generated a larger separation between vitelline membrane and the embryo which increased image quality. Before their use in downstream staining, embryos were rehydrated through a series of methanol/PBTw dilutions (75%, 50%, 25%), and finally washed three times in PBTw. After removing the PBTw, embryos were incubated with a single drop of VectaShield mounting medium with DAPI (Vector Laboratories) for 10 min at 4°C in the dark. Fixed DAPI counterstained embryos were transferred along with the mounting media onto a microscope slide, covered with a cover slip and imaged.

2.3 | Hybridization Chain Reaction

For embryonic florescent in situ hybridization experiments, embryos were not treated with bleach during the fixation process. Instead, the chorion was manually removed, and

the vitelline membrane was left intact for pregastrulation stage embryos. For embryos after gastrulation, the vitelline membrane was removed manually. *M. pharaonis nanos* and *oskar* mRNA were visualized using the Hybridization Chain Reaction (HCR) method (Choi et al. 1987 Molecular Instruments). For *nanos*, 20 probes were generated against *M. pharaonis nanos* (XM_012677141). For *oskar*, 20 probes were generated against *M. pharaonis oskar* (XM_012677375). Hybridization chain reaction was performed using the manufacturer's buffers and protocols (Choi et al. 1987; Molecular Instruments).

For wholemount fluorescent in situ hybridization of larvae, HCR was performed following the whole-mount Drosophila HCR v3.0 protocol (Choi et al. 2018) with some modifications. *M. pharaonis* larvae were fixed at room temperature in scintillation vials with 50% FPE (4% formaldehyde; 0.5× PBS; 25 mM EGTA) and 50% heptane. Fixation time was then adjusted so that 1st and 2nd larval instars were fixed for 2–3 h, and 3rd larval instars were fixed for 12 h. Following fixation, the lower layer (FPE) was removed and replaced with methanol followed by vigorous shaking. The lower layer was replaced once more with methanol, at which point larvae sink to the bottom of the vial. Larvae were then dehydrated with several changes of methanol and stored at −20°C. Proteinase K concentration and treatment time was adjusted to 50 μg/mL for 7 min for 1st and 2nd larval instars and 60 μg/mL for 7 min for 3rd larval instars. Following amplification, one SSCT wash (5× SSC; 0.1% Tween-20; pH 7.0) was extended overnight with the addition of SYTOX Deep Red (1:1000) for nuclear staining in 1st, 2nd, and 3rd larval instars. For *vasa*, 20 probes were generated against *M. pharaonis vasa* (XM_012686851.3). For *headcase*, 20 probes were generated against *M. pharaonis headcase* (XM_036286481.1).

2.4 | Antibody Staining

Cellular blastoderm embryos were fixed and dissected as discussed above. Antibody staining was done as described in Rafiqi, Rajakumar, and Abouheif (2020). Rabbit anti-Vasa antibody (gift from Paul Lasko) was used at a concentration of 1:100. Anti-rabbit Alex Flour 555 secondary antibody (Cell signaling, #4413) was used at a concertation of 1:500.

2.5 | Imaging

For embryos, DAPI images were captured at 20× magnification on an upright Olympus BX63F fluorescence microscope (Tokyo, Japan) equipped with a Retiga 6000 camera system (Qimaging, Surrey, British Columbia, Canada) using cellSens Dimension software version 1.16. For each embryo, a series of Z-stack images were acquired (step), going from one side to the other. Z-stack images were then deconvolved (Gaussian) and only relevant stacks were selected to create either a maximum or an average intensity projection z-stack image. Images were further processed in Adobe Photoshop CC to optimize brightness and contrast.

For brightfield images and videos of embryos, eggs were collected from the stock colony using a fine brush, placed on a microscope slide and gently covered with a cover slip. Drops of halocarbon oil 700 (Sigma-Aldrich) were released on the side of the cover slip and capillary action allowed the oil to slowly displace air and submerge the eggs. Eggs were not dechorionated. Lastly, for brightfield embryo images (Figure 4), embryos were processed in Adobe Photoshop 2021 by changing brightness and contrast, along with sharpening the image, which allowed visualization of cell contours within the blastoderm. Eggs were imaged using the same protocol described for DAPI counterstained embryos. For videos, pictures were taken at different focal points every 20 min at room temperature.

For HCR-stained embryos, embryos were imaged using a Leica SP8 confocal microscope. Images are presented as maximum intensity Z-stacks, which were compiled using ImageJ2 (Rueden et al. 2017).

For brightfield images of whole larvae to make the images less distracting we subtracted the background to make the larvae over a black background (Figure 6).

For wholemount HCR-stained larvae, larvae were transferred into increasing concentrations of glycerol in 5× SSC and mounted in ProLong Glass Antifade Mountant for imaging. Images were captured on a Leica STELLARIS 8 inverted confocal laser scanning microscope. Image stacks were processed using Fiji/ImageJ (Rueden et al. 2017).

For imaging of pupae, pupal developmental series were obtained by isolating prepupae stages of reproductives and workers in Fluon coated petri dishes. As soon as the individuals pupated, they were imaged on consecutive days using the same equipment and procedure as described for larvae and prepupae image acquisition.

2.6 | Larvae and Prepupae Measurements

Larvae and prepupae images were acquired using a BK plus lab system (Dun Inc., Virginia, USA) equipped with a Canon 7D camera. Z-stack images were taken for each individual and combined using the software Zerene Stacker Professional edition. Adobe Photoshop CC was used to measure the maximum cephalic capsule and larval length. Larvae for initial instar identification were collected based on morphological traits previously used in the literature for instar classification (hair types and their presence/absence; mandible coloration) (Berndt and Eichler 1987; Alvares, Bueno, and Fowler 1993).

In total, 340 individuals were collected and classified as follows: 103 1st instars (62 from queenless colonies and 41 from queenright colonies), 51 2nd instar workers, 55 3rd instar workers, 35 prepupa workers, 22 2nd instar reproductives, 50 3rd instar reproductives, and 24 prepupa reproductives. The $\log_{10}$ of both measurements were then plotted to confirm whether collecting larvae using previously described morphological criteria produces distinct clusters corresponding to larval instars.

If the number of larval instars that we annotated is correct, then the growth between instars should be relatively constant. To test this, the growth ratios between successive instars were calculated using the Brooks–Dyar rule, which estimates if the growth ratios between instars are relatively constant or not (Brooks 1886; Dyar 1890; Resh and Cardé 2009; Sukovata 2019). The following equation was calculated:

$$g_i = \mu_i/\mu_{(i-1)}$$

Here, g_i is the Brooks–Dyar ratio, μ_i is the mean head width of a given instar, and $\mu_{(i-1)}$ is the mean head width for the preceding instar. Once the Brooks–Dyar ratio is obtained for successive instars, they are used to calculate Crosby's growth ratio (C_i), which indicates the percentage difference in growth rate between instars. This was calculated using the following equation:

$$C_i = 100(g_i - g_{(i-1)})/g_{(i-1)}$$

Here, a difference in the change of growth exceeding ±10% between successive growth ratios indicates that the annotated instars do not conform to the Brooks–Dyar rule. If C_i is greater than 10% this indicates that one or more instars may be missing and when C_i is greater than −10% this indicates that there may be too many annotated instars. Following this analysis, 235 additional larvae were sampled (49 larvae from queenright colonies and 186 from queenless colonies) and measured to see if individuals filled in the morphospace between the putative 1st instar and 2nd worker instar or between the 2nd worker instar and the 2nd reproductive instar.

2.7 | SEM Microscopy

Representative instar larvae were collected from the two subcolonies used for larval collection and imaged using an environmental scanning electron microscope (FEI Inspect S SEM, Thermo-Fisher Scientific). Images were taken in a low vacuum, at an accelerating voltage of 7 kV.

3 | Results and Discussion

3.1 | Embryonic Development

Under our experimental conditions (see Materials and Methods), *M. pharaonis* embryonic development lasts approximately 10 days. There are 17 embryonic stages in the fruit fly *Drosophila melanogaster* (Campos-Ortega and Hartenstein 1985). Using bright-field microscopy (Figure 2), DAPI-stained embryos (Figures 3 and 4), and brightfield time-lapse videos of living embryos (Embedded Video 1), we identified homologous developmental events in *M. pharaonis*. This allowed us to annotate 17 developmental stages of *M. pharaonis* embryogenesis and harmonize them with those described by Campos-Ortega and Hartenstein (1985) for *D. melanogaster*. For stage durations (hours after egg-laying) and sample sizes see Table 1 and Table 2. These 17 developmental stages are as follows.

TABLE 1 | Sampling scheme of *Monomorium pharaonis* embryos for staging. Left column: Time intervals that eggs were collected following the isolation of *M. pharaonis* queens. Middle column: The number of embryos fixed, DAPI stained and staged at a given time period. Right column: The stages represented during this time window.

Time interval (hours)	Number of embryos	Stages identified
0–6	32	1
6–12	32	2
12–18	41	2, 3
18–24	28	3, 4
24–27	17	4, 5
24–30	137	4, 5
27–30	34	5
30–33	16	5
30–36	40	5
36–42	77	6
42–48	120	7
48–54	24	8
54–60	10	8
60–66	39	8
66–72	40	9
72–84	44	9, 10
84–96	50	10
96–108	83	11
108–120	27	11
120–132	19	11
132–144	78	11
144–156	55	11
156–168	48	11
168–180	46	12
180–192	31	12
192–204	16	13
204–216	14	14, 15
228–240	28	16, 17
Total	**1226**	

3.1.1 | Stage 1, Syncytium

(*0–6 h after egg laying* [*HAEL*]). Freshly laid eggs are 292 ± 21 μm long and 187 ± 18 μm wide (mean ± SD, $n = 36$). The anterior pole is narrower and more rounded than the posterior pole (Figure 2a). Four female meiotic products are located near the anterior part of the egg cytoplasm. Upon fertilization, one of the four female meiotic products (the future female pronucleus) and the male pronucleus localize together in the interior of the egg ("PN", Figure 3a) and later fuse to form the first zygotic nucleus, like *D. melanogaster* (Kotadia et al. 2010). The other three female meiotic products (polar bodies "Pb", Figure 3a) remain in the cortical region of the egg

TABLE 2 | Sample size of *Monomorium pharaonis* embryos for a given stage. Left column: Stage classified after DAPI staining. Right column: Total number of embryos we examined at a given stage.

Embryonic stage	Total number of embryos
1	32
2	73
3	69
4	182
5	244
6	77
7	120
8	73
9	84
10	94
11	310
12	46
13	16
14	14
15	14
16	28
17	28

(Kotadia et al. 2010). Under bright-field microscopy, the yolk appears fine and uniform in color and a small empty space is visible between the vitelline membrane and the egg cytoplasm at the posterior pole (Figure 2a). Stage 1 lasts until the end of the first two cleavage divisions, with the resulting four zygotic nuclei located in the center of the yolk (Figure 3b).

3.1.2 | Stage 2, Syncytium

(*6–16 HAEL*). In *D. melanogaster*, Stage 2 starts at the beginning of the 3rd cleavage cycle and terminates at the end of the 8th cleavage cycle, when the embryo consists of a syncytial blastoderm of 256 nuclei. The first synchronous nuclear divisions occur in the central part of the yolk, until 64 nuclei are formed (Figure 3c). Under bright-field microscopy, the yolk is now lighter in color as the syncytial nuclear divisions progress (compare Figure 2a,b). The synchronized nature of the nuclear divisions can be observed in DIC time-lapse of living embryos, as each division leads the embryo to expand and contract rhythmically (Embedded Video 1, seconds 2–4).

3.1.3 | Stage 3, Syncytium to Syncytial Blastoderm

(*16–20 HAEL*). In *D. melanogaster*, Stage 3 spans the period between the last nuclear divisions and the arrival of the nuclei at the surface of the yolk (Figures 2c and 3d, and Embedded Video 1, second 5). The distribution of the nuclei at the periplasm is uniform. However, unlike in *D. melanogaster*, there is no indication of morphologically distinct pole cells at the posterior pole (Figures 2c and 3d).

3.1.4 | Stage 4, Syncytial to Cellular Blastoderm

(*20–25 HAEL*). In *D. melanogaster*, Stage 4 is characterized by the formation of the blastoderm. During this stage, the first breaking of symmetry between the dorsal and ventral axis of the embryo occurs (Figure 3e and Embedded Video 1, seconds 6–7). The blastoderm nuclei (white) concentrate toward the ventral-lateral side of the posterior pole, whereas nuclei in the dorsal region are sparse. Moreover, under bright-field microscopy, the cells in the dorsal-anterior region appear to be larger than those in the forming embryo primordia, termed the "germ disc" (Figure 2d). Therefore, based on both the increased distance between nuclei and the size of cells within this region, we propose these cells are the developing extraembryonic region of the embryo (hereafter "presumptive extraembryonic region": "Ee"). However, genetic markers, such as *zen* and *dpp*, will be required to confirm the identity of these cells and determine the exact boundaries between the extraembryonic nuclei and germ disc (Panfilio 2008;

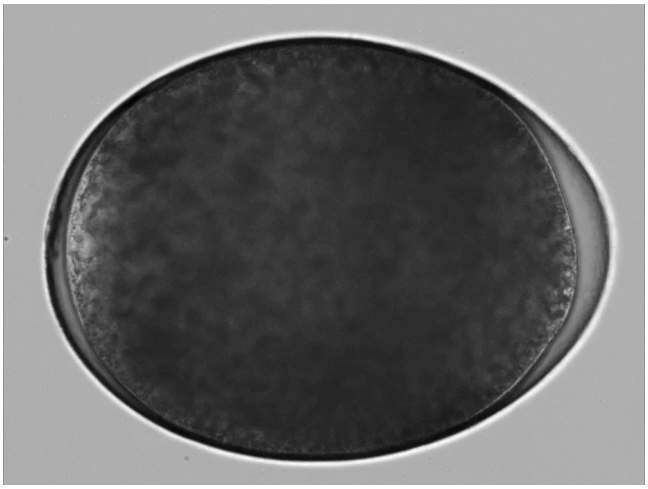

VIDEO 1 | Live imaging of *M. pharaonis embryogenesis.* AVI, Live imaging spans from egg deposition (Stage 1) through gastrulation and germ band extension (Stage 9).

Rafiqi et al. 2008). Finally, the beginning of cellularization is apparent (Figure 2d), although a membrane marker will be required to confirm whether cellularization is partial or complete.

3.1.5 | Stage 5, Cellular Blastoderm

(*25–36 HAEL*). In *D. melanogaster*, Stage 5 is characterized by the completion of cellularization of the blastoderm. In *M. pharaonis*, there is further aggregation of the germ disc toward the ventro-posterior side of the egg (Figure 3f), as well as an extension of presumptive extraembryonic region from the dorsal-anterior side of the egg to both the ventral-anterior and posterior pole ("Ee" in Figure 3f). Furthermore, a series of morphogenetic movements in the dorsal and postero-ventral regions can be observed (Embedded Video 1, seconds 8–17). First, a posterior-ventral fold forms (compare black arrowheads in Figure 2e–f and Embedded Video 1, seconds 9–11). From the dorsal view of the embryo, germ disc nuclei at the posterior pole are absent and instead there is a presumptive extraembryonic region along the entire anterior–posterior axis (Figure 4j). Second, as Stage 5 progresses, the germ disc extends back toward the posterior pole (compare white asterisks and arrowheads in Figure 4a–b and compare Figure 4j–k). Later, the dorsal–posterior region of the embryo shifts anteriorly, and the anterior side of the embryo separates from the vitelline membrane, creating a more compact embryo (Embedded Video 1, seconds 9–18).

3.1.6 | Stage 6, Cellular Blastoderm to Gastrulation

(*36–42 HAEL*). In *D. melanogaster*, Stage 6 encompasses gastrulation. In *M. pharaonis*, from the ventral view, there are apparent changes within the germ disc where the presumptive ectodermal plates seemingly break contact with the presumptive mesoderm ("EP" and "M" in Figure 4c). The break in contact between the ectodermal plates and the presumptive mesoderm can be distinguished by two strips of more loosely organized cells (cyan lines in Figure 4c). However, genetic markers such as *sog* and *twist* will be required to determine the exact boundaries between ectoderm and mesoderm (Stathopoulos and Newcomb 2020). Furthermore, during this stage, the space between the anterior pole of the egg and the anterior of the germ disc decreases, as the anterior of the germ disc extends anterodorsally (compare yellow brackets in Figure 4a–c). In the lateral position, the germ disc becomes more organized forming a wedge that takes up about 2/3 of the egg, while the presumptive extraembryonic region makes up the rest of the egg (Figure 2g, "Ee" in Figure 3g). Finally, the space between the embryo and the anterior of the vitelline membrane increases, making the embryo more compact (Embedded Video 1, 19–29 s).

3.1.7 | Stage 7, Gastrulation to Germ Band Extension

(*42–48 HAEL*). In *D. melanogaster*, Stage 7 is characterized by the end of gastrulation and initiation of germ band elongation. *M. pharoanis* also undergoes both processes at this stage, but unlike *D. melanogaster*, gastrulation proceeds with no signs of mesoderm invagination (Figure 4d). Instead, it appears as though the ectodermal plates slide over the mesoderm resulting in its internalization (compare cyan line in Figure 4c–d). This is further evidenced by looking at both ventral and dorsal views, where germ disc nuclei become absent from the lateral sides of the egg (compare Figure 4b–d and compare Figure 4k–l; asterisks denote the absence of presumptive ectoderm). This suggests that the presumptive lateral ectoderm shifted ventrally. During this stage, germ band elongation initiates, where the posterior end of the germ disc extends along the dorsal side of the egg (Figure 2h, compare white arrowheads in Figures 3g–h, 4k–l, and Embedded Video 1, 30–37 s). As a result, the presumptive extraembryonic region is shifted toward the antero-dorsal compartment of the egg ("E" in Figure 3h). From the ventral view, as the germ band extends toward the anterior pole of the egg, the space between the embryo and the anterior of the egg becomes almost completely closed (compare yellow brackets in Figure 4c–d).

Gastrulation itself in *M. pharaonis* appears to follow the "hymenopteran type", first reported in *Apis melifera* (Fleig and Sander 1986, 1988) and further described by Lynch, El-Sherif, and Brown (2012) in *Nasonia vitripennis*. For example, the blastoderm cells located in the dorsal and lateral sides move in a ventral direction, forming a compact epithelium covering the ventro-lateral regions of the blastoderm (compare Figure 4b–d). This movement leaves very few blastoderm nuclei at the dorsal region (Figure 4l). The morphology of the dorsal region appear to be similar to the "dorsal strip" characterized in *A. mellifera* (Fleig and Sander 1986).

3.1.8 | Stage 8, Germ Band Extension

(*48–66 HAEL*). In *D. melanogaster*, Stage 8 is characterized by the continuation of germ band elongation. In *M. pharaonis*, the extension of the germ band toward the dorsal side of the egg continues (Figures 2i and 3i, Embedded Video 1, 38 s to 1 min 30 s). As the anterior end of the germ band shifts dorsally, the posterior end of the germ band shifts slightly ventrally from its maximal dorsal position in Stage 7, resulting in a symmetrical embryo (compare white arrowheads in Figure 3h–i). Unlike in Stage 7, where only the posterior end of the germ band is at the dorsal side of the egg, in Stage 8, both anterior and dorsal ends of the germ band are dorsal (compare asterisks and white arrowheads in Figure 4l–m). On the ventral side, the germ band narrows, presumably because the ectoderm plates have now completely slid over the mesoderm following gastrulation in Stage 7 (Figure 4e). Furthermore, at the surface of the ventral view there is a narrow overlay of ectoderm ventral to the mesoderm (white arrowheads in Figure 4e). We infer this to be the presumptive mesectoderm. However, this would require confirmation with a genetic marker, such as expression of the *single-minded* gene (Stathopoulos and Newcomb 2020).

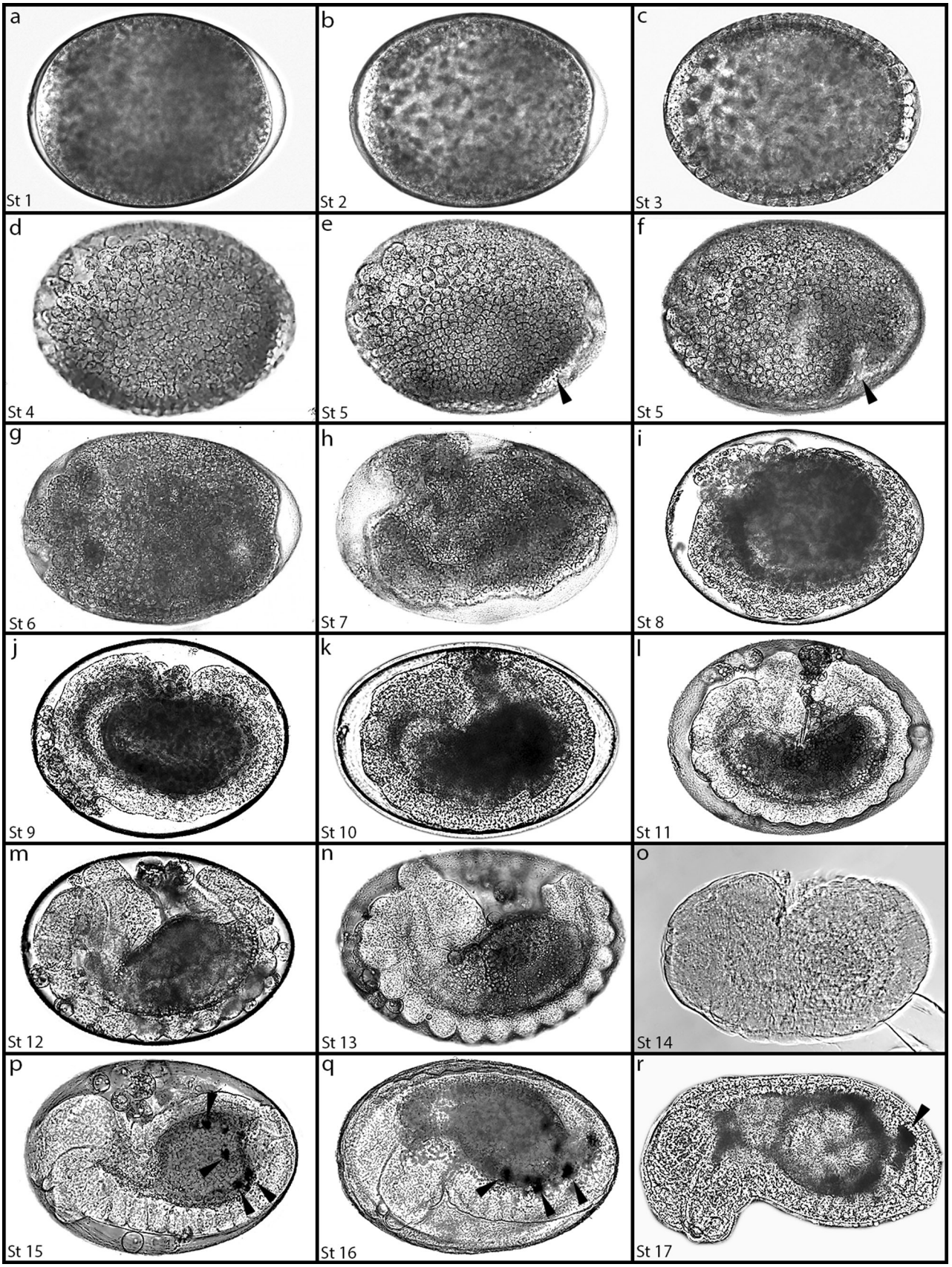

FIGURE 2 | Legend placed on page 568.

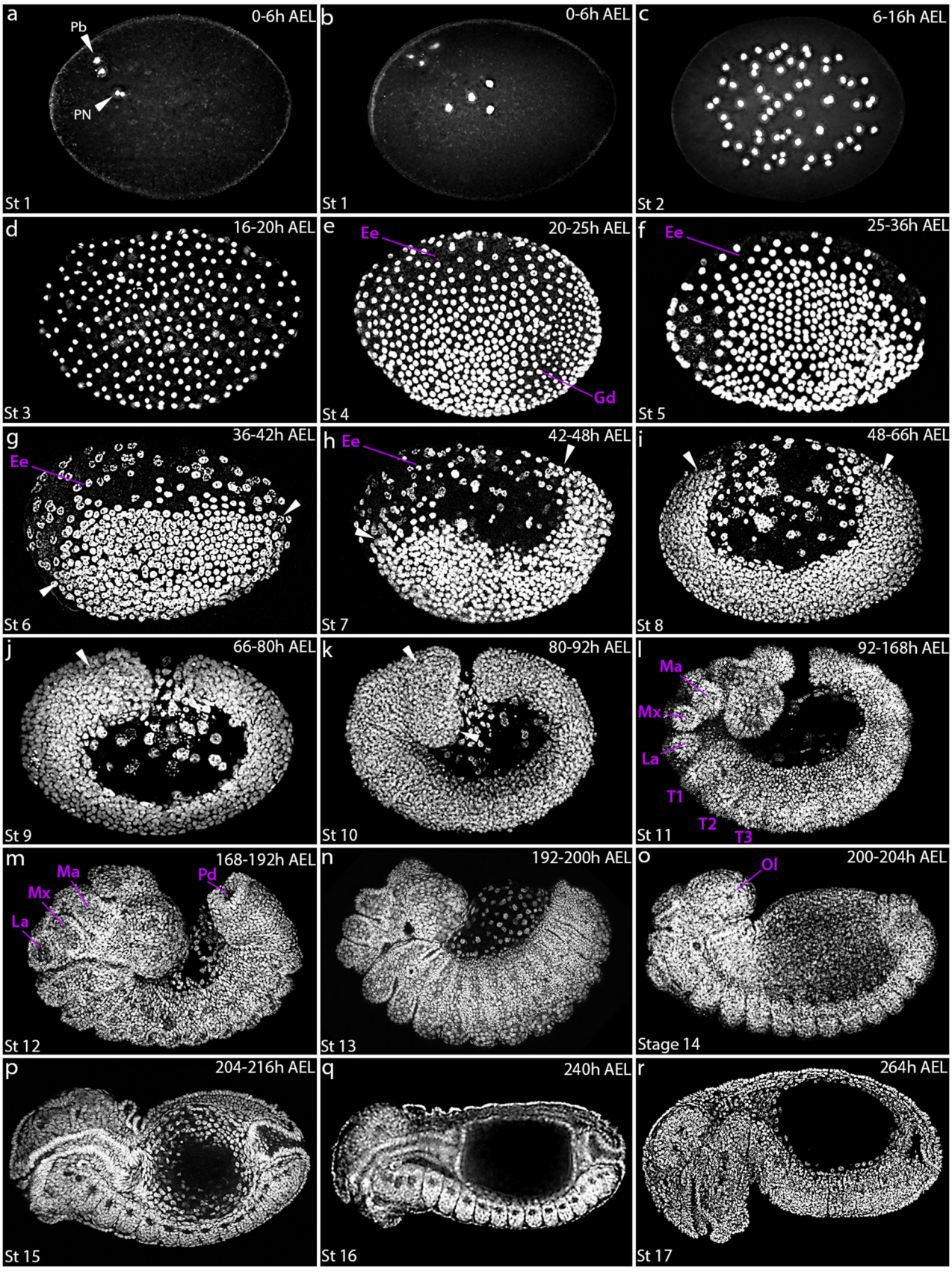

FIGURE 3 | Legend placed on page 568.

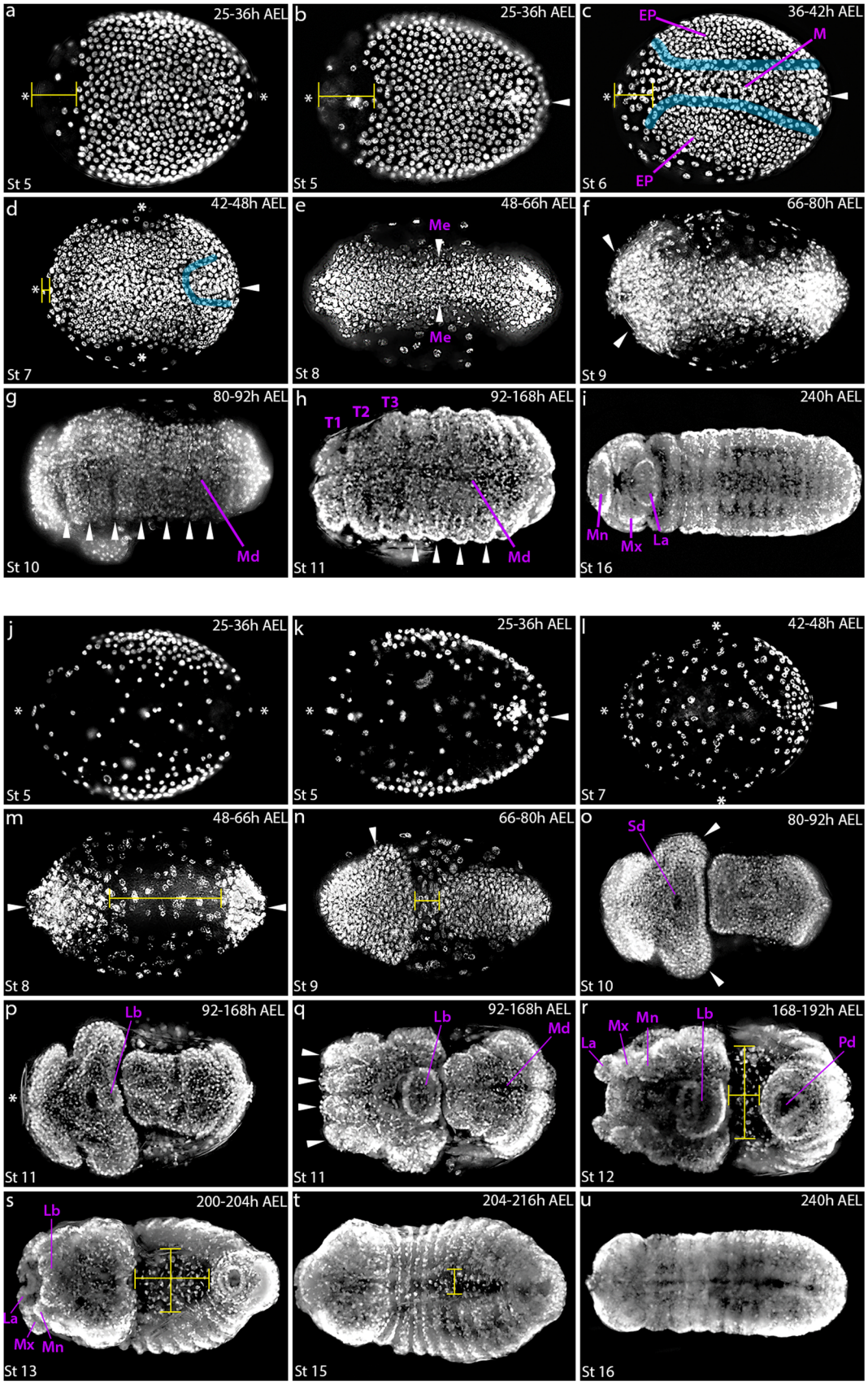

FIGURE 4 | Legend on next page.

3.1.9 | Stage 9, Germ Band Extension

(*66–80 HAEL*). In *D. melanogaster*, Stage 9 is characterized by the completion of germ band extension. In *M. pharaonis*, the germ band has reached its maximum extension and it now covers the dorsal side of the egg (Figures 2j and 3j, Embedded Video 1, 1 min 31 s to 1 min 39 s). From the dorsal view, the gap between the anterior and posterior ends of the germ band is almost closed (compare yellow brackets in Figure 4m–n). Furthermore, both ventral and dorsal views reveal that the head anlage is beginning to develop at the anterior of the germ band, where the anterior end becomes markedly thicker than the posterior of the germ band (compare white arrowheads in Figure 4f–n).

3.1.10 | Stage 10, Segmentation

(*80–92 HAEL*). In *M. pharaonis*, Stage 10 is characterized by continued development of the germ band (Figures 2k and 3k). From the dorsal view, the anterior and posterior ends of the germ band are now in contact (Figure 4o). Both lateral and dorsal views show a significant increase in the size of the head anlage (compare white arrowheads in Figure 3j–k and in Figure 4n–o). Moreover, from the ventral view, we observe a series of grooves running perpendicularly to the embryonic midline, thereby establishing boundaries between germ band segments (white arrowheads in Figure 4g). Finally, the stomodaeum (precursor of the mouth) arises as an ovoidal invagination ("sd", Figure 4o).

FIGURE 2 | Brightfield images of *Monomorium pharaonis* embryonic stages. (a–r) Staging table (St) of embryos imaged with brightfield microscopy. *M. pharaonis* embryonic stages were harmonized to the 17 stages (St) of *D. melanogaster*. (a, b) St 1–2: syncytial blastoderm stages. (c) St 3: Blastoderm stage, note change in morphology at the egg cortex. (d–f) St 4–5: Cellular blastoderm. Note, cell boundaries are visible at the egg surface. Black arrow indicates the formation of the ventral-posterior fold. (g, h) St 6–7: Gastrulation stages. (i–k) St 8–10: germ band extension stages. (l) St 11: segmentation stage. (m, n) St 12–13: germ band retraction stages. (o, p) St 14–15: dorsal closure stages. (q) St 16: embryo straightens. (r) St 17: end of embryogenesis. (p–r) Black arrows indicate the presence of black puncta, which may be oenocytes. Anterior is to the left, posterior is to the right, dorsal is up, and ventral is down.

FIGURE 3 | Embryonic stages of *Monomorium pharaonis* development. (a–r) Staging table of embryos stained with DAPI, which marks DNA. (a–c) St 1–2: syncytial nuclear divisions. (d) St 3: blastoderm stage. (e, f) St 4–5: cellular blastoderm stages. (g, h) St 6–7: gastrulation stages. (i–k) St 8–10: germ band extension stages. (l) St 11: segmentation stage. (m, n) St 12–13: germ band retraction stages. (o, p) St 14–15: dorsal closure stages. (q) St 16: embryo straightens. (r) St 17: end embryogenesis. Arrows in (a) indicate polar bodies (Pb) and pronuclei (Pn). Arrows in (g–i) indicate anterior and posterior end of the germ disc to highlight their movements along the dorsal side of the egg. Arrows in (j, k) are to highlight development of the head segment. (e–h) Presumptive extraembryonic region (Ee). AEL = after egg laying, Gd = germ disc, Mn = mandible, Mx = maxilla, La = labium, Pd = proctodeal invagination, T1 = 1st thoracic segment, T2= 2nd thoracic segment, T3 = 3rd thoracic segment, Ol = optic lobe. Embryos are in a lateral position. Anterior is to the left, posterior is to the right, dorsal is up, and ventral is down.

FIGURE 4 | Ventral and dorsal views of *Monomorium pharaonis* germ band development. (a–i) Ventral-orientated embryos stained with DAPI. (a, b) Stage (St) 5: cellular blastoderm stage embryos, asterisks highlight the absence of germ disc nuclei at the anterior or posterior pole. Arrow in (b) highlights the arrival of germ disc nuclei to the posterior pole. (c) St 6: gastrulation stage. EP = presumptive ectodermal plates; M = presumptive mesoderm. Cyan line highlights the break in contact between the ectodermal plates and the mesoderm at the start of gastrulation. (d) St 7: gastrulation stage. Asterisks along the middle length of the egg highlight empty space on the two lateral sides of the embryo as the ectodermal plates shift the ventral side of the embryo, which is consistent with the shortening of the area marked by a cyan line. (a–d) Yellow brackets highlight the gradual anterior movement of the germ disc between cellular blastoderm and gastrulation stages. (e) St 8: germ band extension stage. Arrows indicate the presumptive Mesectoderm (Me). (f) St 9: germ band extension stage. White arrows indicate the developing head segment. (g) St 10: germ band extension stage. White arrow grooves that appear to separate segment boundaries perpendicular to the ventral midline (Md). (h) St 11: segmentation stage. Arrows indicate formed segments perpendicular to the ventral midline (Md). T1 = 1st thoracic segment, T2 = 2nd thoracic segment, T3 = 3rd thoracic segment. (i) St 16: embryo. Gnathal segments are in the ventral direction as the embryo straightens. Mn = mandible; Mx = maxilla; la = labium; pd = proctodeal invagination. (j–u) Dorsal-orientated embryos. (j) St 5: cellular blastoderm embryo. Asterisks indicate the absence of germ disc nuclei from the anterior or posterior pole. (k) St 5: cellular blastoderm stage. White arrow indicates the movement of germ disc nuclei to the posterior pole. (l) St 7: gastrulation stage. White arrow indicates a thicker layer of cells at the posterior pole. Asterix along the middle length of the egg indicates that the ectoderm has shifted toward the ventral side. (m) St 8: germ band extension stage. White arrows indicate germ disc nuclei are now at both poles. Thickness of nuclei rows indicates that the germ band is extended to the dorsal side of the egg at both poles. (n) St 9: germ band extension stage. White arrow indicates the development of the head anlage. (o) St 10: germ band extension stage. White arrows highlight further development of the head anlage. The stomodaeum (Sd) is now visible. (m–o) Progression of germ bang extension. Horizontal yellow brackets highlight the closing of the gap between the anterior-most and posterior-most ends of the germ band. (p,q) St 11: segmentation stage. (p) Early St 11 embryo where the labrum is now visible to the posterior of the stomodaeum. (q) Late St 11 embryo highlighting more developed labrum and formation of the gnathal segments (white arrows). (r) St 12: germ band retraction stage. (s,t) St 13–15: dorsal closure stages. (r, s) Horizontal yellow bracket indicates the progression of germ band retraction. (r–t) Vertical yellow bracket indicates progression of dorsal closure. (u) St 16: straightening stage. Embryo has straightened and the gnathal segments are no longer visible. Anterior is to the left and posterior to the right.

3.1.11 | Stage 11, Segmentation

(*92–168 HAEL*). In *D. melanogaster*, Stage 11 is characterized by the completion of segmentation, where all segments of the embryo become well defined. In the lateral view, the gnathal segments in *M. pharaonis* (mandible "Mn", maxilla "Mx", and labium "La") are well defined as rounded bulges, while the thoracic and abdominal segments are less pronounced (Figure 3l). Moreover, the thoracic segments (T1, T2, and T3) are more easily discernible than the abdominal segments (Figure 3l). However, by viewing the embryo from the ventral side, the pronounced ridges between abdominal segments are more discernible (arrowheads in Figure 4h). Furthermore, bright-field microscopy shows the segmentation through the entire embryonic abdomen even more clearly (Figure 2l). Moreover, the ventral midline is now visible ("Md" in Figure 4h). From the dorsal view, the head anlage develops more pronounced folds (Figure 4q). Specifically, the stomodaeum deepens, and the labrum begins to form as an ovoid protrusion of tissue immediately anterior to the stomodaeum ("Lb" in Figure 4p). As Stage 11 progresses, the gnathal segments continue to develop (compare the asterisk in Figure 4p with arrowheads in Figure 4q).

3.1.12 | Stage 12, Germ Band Retraction

(*168–192 HAEL*). In *D. melanogaster*, Stage 12 is characterized by the start of germ band retraction. In *M. pharaonis*, the distance between the posterior end of the germ band from the posterior end of the head anlage widens (Figures 2m and 3m, horizontal yellow bracket in Figure 4r). During this stage, the gnathal segments appear elongated, are oriented upward, and are more condensed (Figures 3m and 4r). Furthermore, the labrum grows significantly (Lb in Figure 4q). Moreover, abdominal segments are now clearly distinguishable when viewing the embryo laterally (Figure 3m). Finally, the proctodaeum becomes visible ("Pd" in Figures 3m and 4r).

3.1.13 | Stage 13, Germ Band Retraction

(*92–200 HAEL*). In *D. melanogaster*, Stage 13 is characterized by the end of germ band retraction and the start of dorsal closure. In *M. pharaonis*, there is a further increase in the gap between the posterior end of the germ band to the posterior end of the head anlage (Figures 2n and 3n, compare horizontal yellow brackets in Figure 4r–s). Conversely, at the onset of dorsal closure, there is a narrowing of the two lateral flanks of the embryo as they grow toward the midline (compare vertical yellow brackets in Figure 4r–s). Finally, the gnathal segments and labrum orient toward the antero-ventral side of the embryo (Figure 2n, compare Figure 4r–s).

3.1.14 | Stage 14, Dorsal Closure

(*200–204 HAEL*). During Stage 14, the gnathal segments are now oriented toward the anterior of the egg, as the head shifts towards the ventral side (Figures 2o and 3o). Optic lobe ("Ol") is now visible in the head (Figure 3o). Dorsal closure proceeds (Figure 3o).

3.1.15 | Stage 15, Dorsal Closure

(*204–216 HAEL*). In *D. melanogaster*, Stage 15 is characterized by the completion of dorsal closure. In *M. pharaonis*, the lateral flanks meet at the dorsal midline to close the dorsal side of the embryo (compare Figure 4s–t). Unlike *Drosophila*, which undergoes head involution, the gnathal segments continue to orient ventrally, and now oriented toward the ventral side in *M. pharaonis* embryos (compare Figure 3o–p). Under bright-field microscopy, small black spots are present in the posterior region of the gut (black arrowheads in Figure 2p). Although a genetic marker would be required to determine the nature of these black spots, based on their morphology and localization in eggs and larvae, we propose that they are oenocytes.

3.1.16 | Stage 16, Straightening

(*10 days after egg laying*). During Stage 16, the embryo straightens (compare dorsal side of the embryo in Figure 2p–q, in Figure 3p–q, and in Figure 4i–u) and the gnathal segments are oriented ventrally (Mn, Mx, and La in Figure 4i). The black dots persist in the posterior of the gut (black arrowheads in Figure 2q).

3.1.17 | Stage 17, Micro Larvae

(*11 days after egg laying*). Stage 17 marks the end of embryogenesis. The fully formed 1st instar larvae outgrow the chorion and hatch (Figures 2r and 3r). The black dots coalesce toward the dorsal posterior of the embryo (black arrowhead in Figure 2r).

3.2 | Germ Cell Specification

Across insects, germ cells are specified via one of two major modes: (1) preformation, in which a specialized cytoplasm called germplasm is maternally deposited into developing oocytes and localized at the posterior pole where germ cells are specified; or (2) induction, in which cell-to-cell signaling induces a group of cells to acquire a germ cell identity later in embryogenesis during segmentation (Extavour and Akam 2003). The macroevolutionary patterns of how different insect lineages specify their germline continues to be elucidated. Within the Hymenoptera, while both modes are present, preformation appears to be more common (Dearden 2006; Khila and Abouheif 2008, 2010; Lynch et al. 2011; Rafiqi, Rajakumar, and Abouheif 2020). To characterize how germ cells are specified in *M. pharaonis*, we used hybridization chain reaction (HCR) to first detect *nanos* mRNA, which marks the germline across animals (Extavour and Akam 2003). In early embryos (Stages 1 and

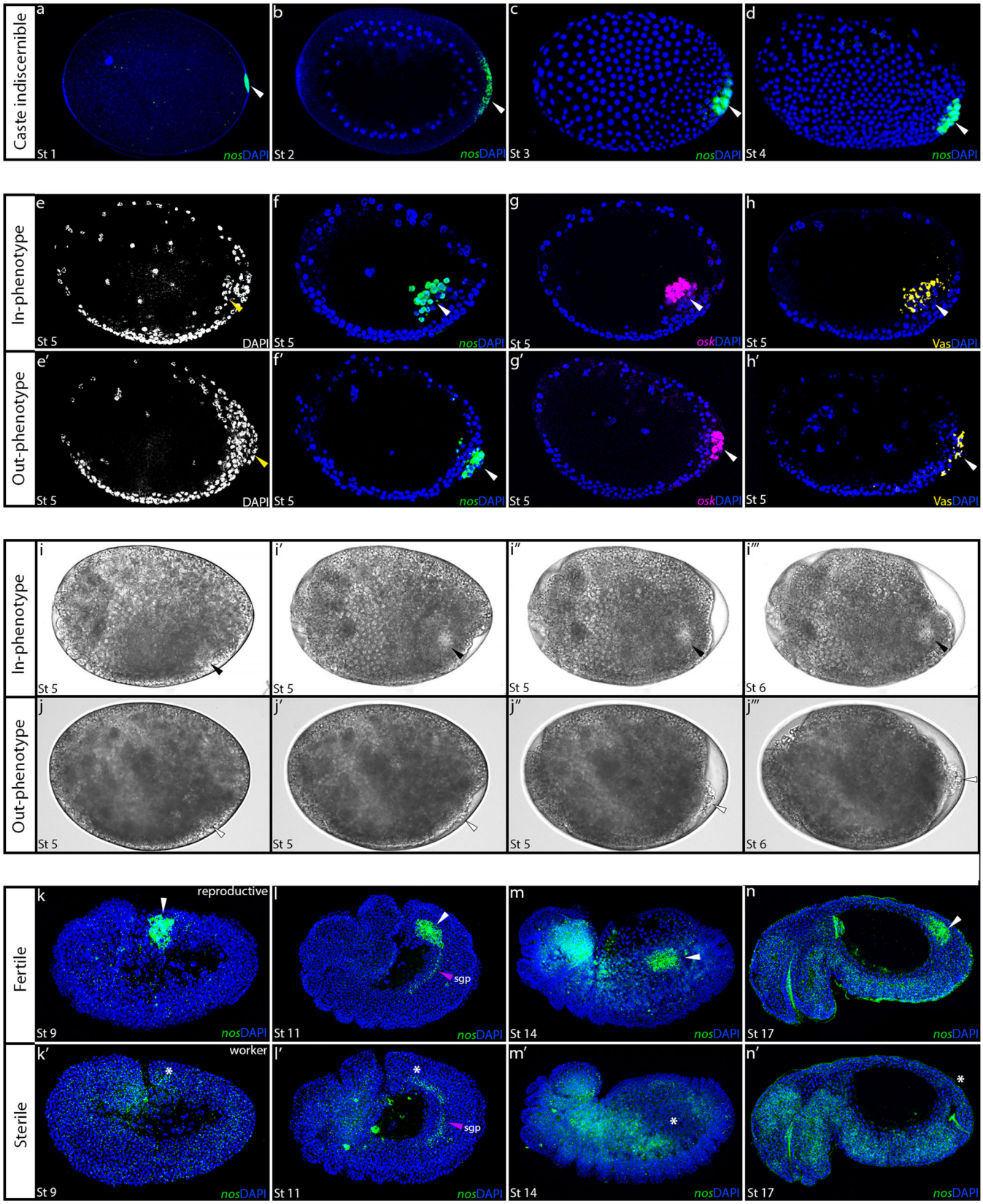

FIGURE 5 | Legend on next page.

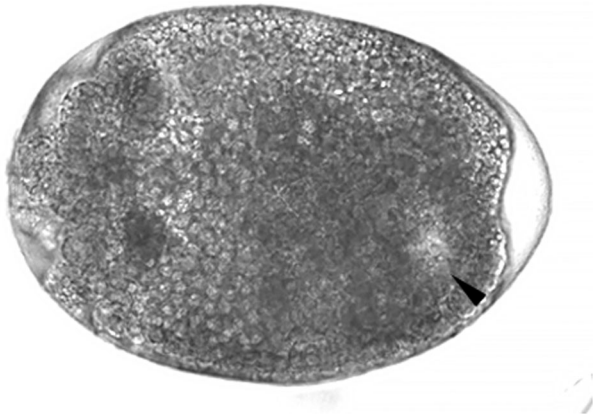

VIDEO 2 | Live imaging of *M. pharaonis* "In"-phenotype embryos. MP4, Live imaging of an "In"-phenotype embryo that spans from cellular blastoderm stage (Stage 5) through the start of gastrulation (Stage 6).

2), we found that *nanos* localizes to the posterior pole marking the germplasm, indicating that *M. pharaonis* specifies its germ cells through preformation like all other ants described to date (Figure 5a,b) (Khila and Abouheif 2008, 2010; Lynch et al. 2011; Rafiqi, Rajakumar, and Abouheif 2020). During Stages 3 and 4, however, when germ cells become extruded from the posterior pole of the embryo in *D. melanogaster*, *M. pharaonis* germ cells are not extruded and remain at the posterior cortex of the embryo (Figure 5c,5d). Surprisingly, during Stage 5 (the cellular blastoderm stage), we discovered two alternative types of germ cell localization in stage-matched *M. pharaonis* embryos (Figure 5e–h'). In one type, the germ cells are located inside the embryo (we call these 'in-phenotype' embryos; $n = 62$; Figure 5e,f), whereas in the alternative type, the germ cells are extruded at the posterior pole (we call these 'out-phenotype' embryos; $n = 124$; Figure 5e',f'). Two additional germline markers, *oskar* mRNA and Vasa protein, strongly mark the germ cells either inside or outside the embryo, confirming the identify of these cell clusters as bonafide germ cells (Figure 5g–h'). To rule out the possibility that in-phenotype and out-phenotype embryos are not successive developmental stages (i.e., in-to-out or out-to-in), we used live imaging to see if we can morphologically distinguish different germ cell migration patterns between embryos. Live imaging confirmed that in-phenotype and out-phenotype embryos are two alternative phenotypes and not successive developmental stages (Figure 5i–j''' and Embedded Videos 2 and 3). For in-phenotype embryos, we did not detect any cells extruded at the posterior pole. Instead, we observed a clearing inside the cellular blastoderm consistent with the internal location of *nanos*-marked germ cells (Figure 5f, black arrowheads in Figure 5i–i''' and Embedded Video 2). For out-phenotype embryos, we detected cells extruded at the posterior pole consistent with the external location of *nanos*-marked germ cells (Figure 5f', white arrowheads in Figure 5j–j''' and Embedded Video 3). Taken together, our results reveal the existence of a germ cell localization polyphenism in early-stage *M. pharaonis* embryos.

M. pharaonis colonies are composed of dozens of queens that are fertile and thousands of smaller-sized workers that are obligately sterile. These workers completely lack a germline and do not develop ovaries. Previous studies on ants have established a general correlation between the degree of size dimorphism between queens and workers and the timing of caste determination within a species. This means that caste determination occurs earlier in development in species with a large queen–worker size dimorphism and later in those species with no or little queen–worker size dimorphism (Passera and Suzzoni 1979; Wilson 1954;

FIGURE 5 | A germ cell migration polyphenism underlies embryonic caste differentiation in *Monomorium pharaonis*. (a–d) Early *M. pharaonis* embryos stained DAPI (blue) and *nanos* (*nos*, green) to reveal germ cell specification. (a) Stage (St) 1: syncytial embryo showing *nos* mRNA in germplasm at the posterior cortex. (b) St 2: syncytial embryo showing nuclei approaching germplasm (*nos* mRNA) at the posterior cortex. (c) St 3: embryo showing initial formation of germ cells (*nos* mRNA). (d) St 4: embryo showing fully specified germ cells at the posterior of the developing germ disc. (e–h') Germ cell polyphenism during cellular blastoderm stage (St 5). in-phenotype (e–h) and out-phenotype (e', f', g', h') embryos stained with DAPI and (e, e'), *nos* mRNA (f, f'), *oskar* (*osk*) mRNA (g, g') or Vasa (Vas) protein (h, h'). i-j''') Live-imaging of in-phenotype and out– phenotype embryos. (i–i''') Successive frame captures of an in–phenotype embryo. Black arrow highlight clearing that coincides with the germ cell cluster. (j–j''') Successive frame captures of an out–phenotype embryo. White arrow highlights cluster of cells extruded for the posterior of the embryo that coincide with the germ cell cluster. Both embryos start at Stage 5 cellular blastoderm stage and end at Stage 6 gastrulation stage. See Embedded Videos 2 and 3 for respective videos. (k–n') Developmental trajectory of germ cells stained with *nos* mRNA in post-gastrulated embryos. (k–n) Fertile embryos with *nos* mRNA marked germ cells (white arrow). (k'–n') Sterile embryos that lack germ cells (asterisks). Note, *nos* mRNA also stains the nervous system and the somatic gonadal precursor cells (sgp, magenta arrow). Anterior is to the left, Posterior is to the right, Dorsal is up, Ventral is down.

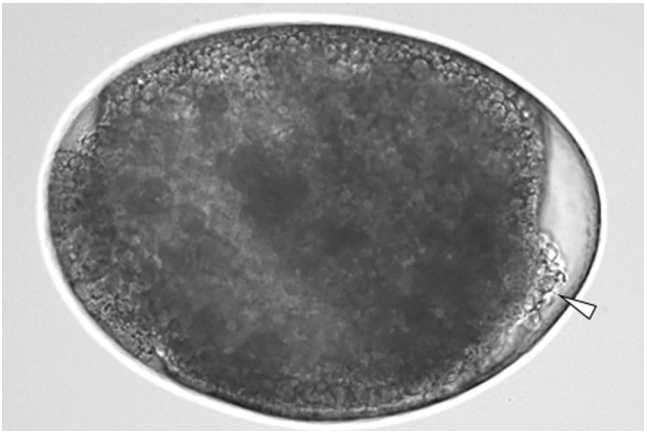

VIDEO 3 | Live imaging of *M. pharaonis* "Out"-phenotype embryos. MP4, Live imaging of an "Out"-phenotype embryo that spans from cellular blastoderm stage (Stage 5) through the start of gastrulation (Stage 6).

Wheeler 1986; Penick, Ebie, and Moore 2013). Consistent with this general correlation, germ cells could not be detected in embryos from another *Monomorium* species, *M. emersoni* (Khila and Abouheif 2010). Therefore, the germ cell localization polyphenism we discovered suggests a caste determination event occurring early in embryogenesis.

To test this hypothesis, we investigated patterns of *nanos* mRNA in mid-to-late-stage embryos (i.e., Stages 8–17) to determine whether we could identify both fertile (embryos with germ cells) and sterile (embryos without germ cells) individuals. From the germ band extension stage (Stage 8) onwards, we found two populations of stage-matched embryos with and without germ cells, confirming the presence of fertile and sterile embryos. Therefore, fertile embryos are reproductive-destined individuals (gyne or male) (Figure 5k–n), whereas sterile embryos are worker-destined individuals (Figure 5k′–n′). Finally, the ratio in-phenotype vs. out-phenotype embryos (n = 62 / 0.33 in-phenotype vs. n = 124 / 0.66 out-phenotype) is within the range for the ratio of adult queens and workers within *M. pharaonis* colonies, which ranges from 0.2 to 0.5 gynes/queens

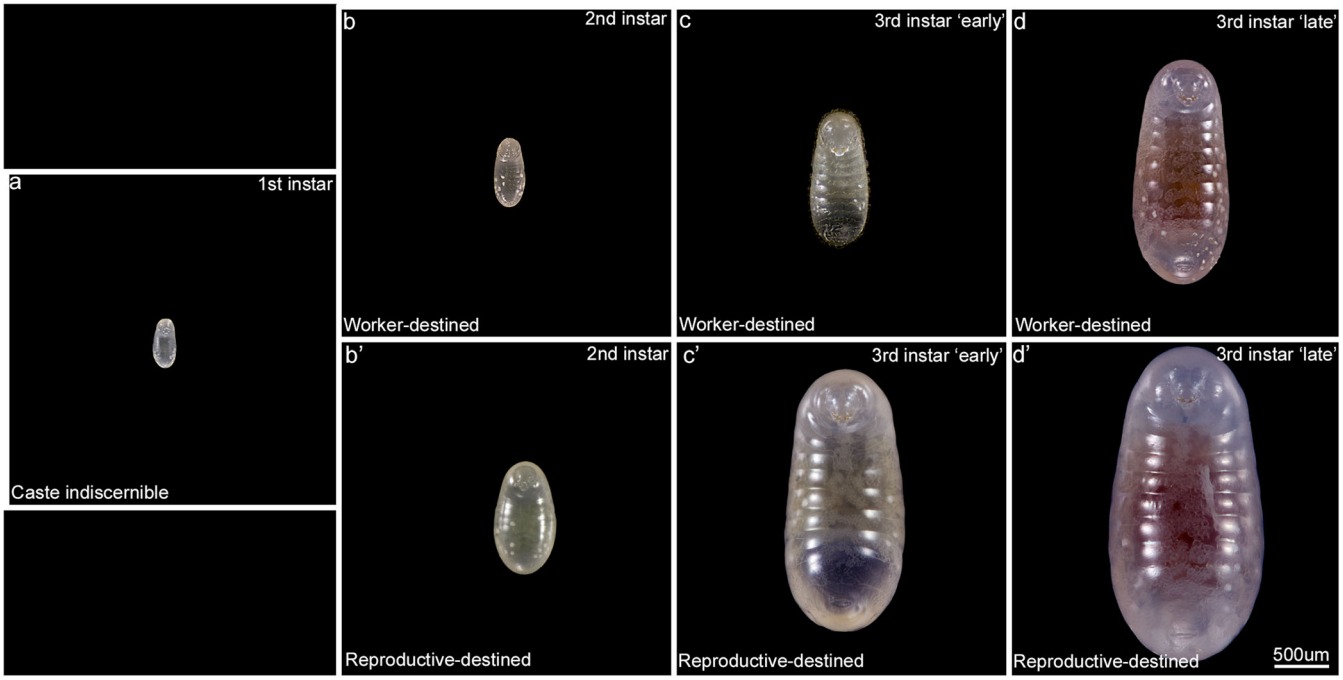

FIGURE 6 | Brightfield images of *Monomorium pharaonis* larval instars. Instar designation is based on Berndt and Eichler (1987) and Alvares, Bueno, and Fowler (1993). (a) 1st instar larvae "Caste indiscernible", where caste is ambiguous based on morphological characters. (b–d) Worker-destined larvae. (b) 2nd instar larvae. (c) 3rd instar larvae "early". (d) 3rd instar larvae "late". (b′–d′) Reproductive-destined larvae. (f) 2nd instar larvae. (g) 3rd instar larvae "early". (h) 3rd instar larvae "late." All images are to scale.

depending on colony size (Schmidt et al. 2010, Warner, Lipponen, and Lisnkvayer 2018). Taken together, our finding of two alternative types of germ cell localization during the blastoderm stage and fertile or sterile embryos later in embryonic development shows that the alternative types of germ cell localization is the earliest known point of caste differentiation between reproductives and workers to date.

3.3 | Larval Development

Under our experimental conditions, larval development in *M. pharaonis* lasts approximately 22 days. Previous studies characterizing the larval development of *M. pharaonis* determined that it proceeds through three larval instars (Figure 6) (Berndt and Eichler 1987; Alvares, Bueno, and Fowler 1993). This characterization was based on using a combination of morphometric measurements, such as head width, body length, diameter of the first thoracic spiracle, and the types and number of cuticular features, such as setae, spines, and tuberculi. It has been shown that the combined use of these traits is sufficient to determine the number of larval instars in several ant species (Masuko 2017). Although Berndt and Eichler (1987) provided thorough descriptions of *M. pharaonis* larvae, they are available only in the German language. Therefore, we provide a brief characterization of the first, second, and three instar larvae of workers and sexuals based on Berndt and Eichler's (1987) descriptions and our own SEM images (Figure 7).

3.3.1 | First Instar Larvae (Caste Not Discernible)

1st instar larvae are slightly longer on the major axis than a freshly laid egg (length ± SD: 0.389 ± 0.032 mm) with an average head width of 0.142 ± 0.006 mm ($n = 103$; Figure 6a). They are whitish in pigmentation and fat with a broader posterior than putative 2nd instar workers (compare Figure 6a–b). The head is ventral at the anterior end, while the anus is postero-ventral (head "Hd", anus "An" in Figure 7a). They have very few cuticular body hairs that are sparse and simple in morphology (Figure 7b). On the ventral side, the prothorax and the abdominal segments bear four short setae, roughly organized in two rows across the ventral midline (setae "St" in Figure 7a,b). The second and third thoracic segments always lack short hairs in the inner row (asterisks in Figure 7a,b), which is a unique trait of this instar. The head is simple, with a slit-like opening at the border between the gena (the lower part of the head that extends behind the maxilla) and the prothorax (white arrowheads, gena "Gn", and prothorax "PTh" in Figure 7a). As the first instar is ready to molt, we observe an increase in the density of hairs and length of setae along the ventral side of the larvae (white arrowhead in Figure 7c).

3.3.2 | Second Instar Larvae (Worker- and Reproductive-Destined Larvae)

This is the first point in development where worker-destined and reproductive-destined larvae are morphologically

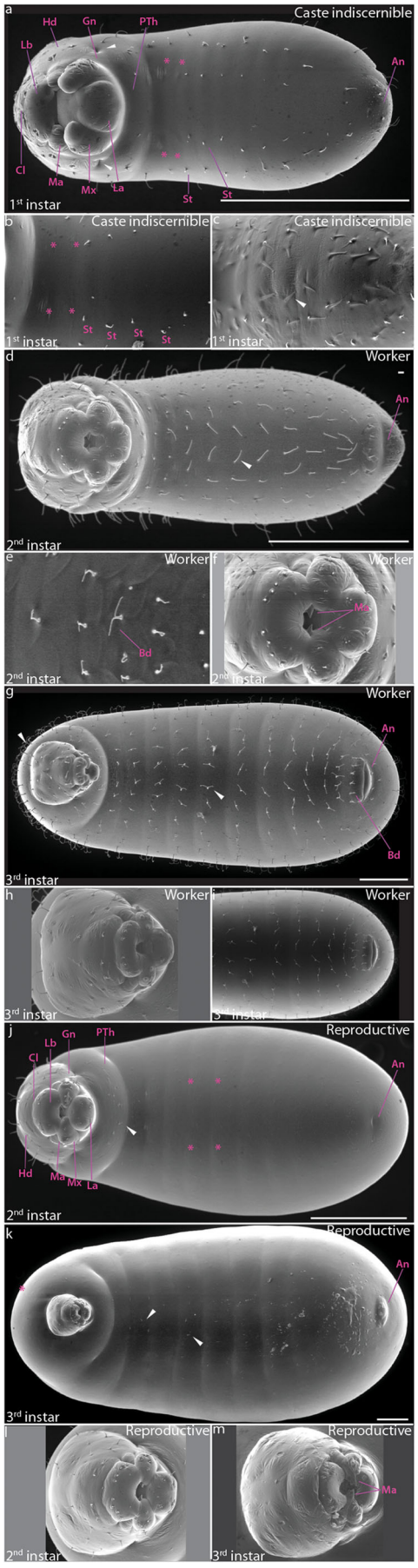

FIGURE 7 | Legend on next page.

discernable (compare Figures 6b–b′ and 7d–j). 2nd instar worker-destined larvae have an average length of 0.572 ± 0.090 mm and an average head width of 0.173 ± 0.008 mm ($n = 51$; Figure 6b). They are whitish in pigmentation and more slender than a 1st instar at the posterior end (compare Figures 6a–b and 7a–d). The location of the anus is sub-terminal (compare Figure 7a–d). We observed numerous long and simple body hairs, rarely bifid (y-shaped), which are mostly uniformly distributed and organized in rows along the segmented body (compare the ventral surface of Figure 7a–d and see bifid "Bd" in Figure 7e). Unlike in the 1st instar, hairs are present on the midline of the ventral surface (compare Figure 7a–d and 7b–e). We observed few simple and sparse hairs on the head (Figure 7d). Compared to the 1st instar, the mandible tooth has become more pointed (compare "Ma" in Figure 7a–f)

Second instar reproductive-destined larvae are whitish in pigmentation and much larger than those of workers with an average length of 1.026 ± 0.192 mm and head width of 0.215 ± 0.004 mm ($n = 22$; compare Figure 6b–b′). They are also larger at the posterior end compared to a 2nd instar worker-destined larvae (compare Figures 6b–b′ and 7d–j). However, unlike 2nd instar worker-destined larvae, there are no hairs on the thoracic and abdominal segments, with the exception of the prothorax that bears a few short simple hairs on the ventral side (white arrowhead and asterisks in Figure 7j). Finally, we observed only a few simple and sparse hairs on the head, organized in a similar fashion to 2nd instar worker-destined larvae (Figure 7j).

3.3.3 | Third Instar (Worker- and Reproductive-Destined Larvae)

Third instar worker-destined larvae have an average body length of 1.551 ± 0.432 mm and an average head width of 0.273 ± 0.009 mm ($n = 55$). They are whitish in pigmentation, but unlike previous instars gut pigmentation and mandibles become increasingly darker as they develop (compare Figure 6b–6c with 6d). Unlike the simple hairs of 2nd instar worker-destined larvae, 3rd instar worker-destined larvae possessed bifurcated and anchor-shaped hairs across the cranium, thoracic, and abdominal segments (compare white arrowheads in Figure 7d–g). Moreover, we observed bifid hairs around the anus (Figure 7g–i). Finally, the clypeus and mouthparts are similar in terms of shape to those described in 2nd instar worker-destined larvae (compare Figure 7f–h).

Third instar reproductive-destined larvae are much larger with an average body length of 2.464 ± 0.397 mm and an average head width of 0.284 ± 0.014 mm ($n = 50$). They are whitish in pigmentation, and like 3rd instar worker-destined larvae, gut pigmentation and the mandibles become increasingly darker with age (compare Figure 6b′ with 6c′ and with 6d′). Furthermore, they are more rotund than 3rd instar worker-destined larvae (compare Figure 6c with 6c′ and Figure 6d with 6d′). Finally, we observed extremely short, straight hairs on thoracic and abdominal segments, which can only be detected using SEM microscopy (Figure 7k). In contrast to 2nd instar reproductive larvae, the cranium possesses almost no hairs and the mandibles are now serrated (compare Figure 7j to 7k and Figure 7l to 7m).

Next, we sought to confirm that *M. pharaonis* worker and reproductive larvae develop over three larval instars by using the same morphological criteria described in Berndt and Eichler (1987) to sample larvae ($n = 340$). We plotted measurements of the maximum head width versus the maximum larval length along the anteroposterior axis (Figure 8a). Our analysis revealed three larval instars for both worker-destined larvae and queen-destined larvae, with the morphospace of the first instar being shared among both (gray dots in Figure 8a). Therefore, using Berndt and Eichler's (1987) sampling criteria, our data confirms the existence of 3 larval instars in *M. pharaonis*, which is consistent with that found for other *Monomorium* species, such as *M. floricola* and *M. trivale* (Berndt and Eichler 1987; Alvares, Bueno, and Fowler 1993; Solis et al. 2010; Idogawa, Gotoh, and Dobata 2022).

Despite our confirmation that *M. pharaonis* has three larval instars, we uncovered that the inter-instar growth rates between worker-destined and reproductive-destined larvae are counterintuitive. Growth between the 1st and 2nd instar is 225% more for reproductive-destined larvae than for worker-destined larvae (72.43 vs. 32.1 μm). In contrast, growth between the 2nd and 3rd instar is 25% less for reproductive-destined larvae than for worker-destined larvae (93.03 vs. 69.98 μm). This finding is counterintuitive because we initially expected that growth would be linear and constantly higher in reproductive-destined larvae as compared to worker-destined larvae to generate the larger body size of gynes (unmated queens), but instead, we found the opposite. Our finding therefore raises the possibility that our characterization of caste-specific developmental trajectories of *M. pharaonis* larvae is incomplete. This may be a problem unique to *M. pharaonis* because larvae of all three castes (i.e., workers, gynes, and males) are produced

FIGURE 7 | SEM images of *Monomorium pharaonis* larval instars. Instar designation is taken from Berndt and Eichler (1987). (a–c) 1st instar larvae, (a) Caste indiscernible), with higher magnification of thoracic region of early first instar, (b) and late first instar, (c) larvae. (d–f) 2nd instar worker larvae (d) with higher magnification of thoracic region of late 2nd instar worker larvae (e) and mouthparts of early 2nd instar worker larvae (f). (g–i) 3rd instar worker larvae (g) with higher magnification of mouthparts of 3rd instar worker larvae (h) and abdominal region of 3rd instar worker larvae (I). (j) 2nd instar reproductive larvae. (k) 3rd instar reproductive larvae. (l, m) Zoomed in images of head and mouthparts of 2nd instar (l) and 3rd instar (m) reproductive larvae. White arrow in (a) indicates a slit-like opening at the border between gena and prothorax. Asterisks indicate the absence of hairs on the inside of the 2nd and 3rd thoracic segments. White arrow in (c) indicates subcuticle hair that will appear after molting. White arrow in (d) indicates long simple hair. White arrow in (g) indicates anchor hair. White arrow in (j, k) indicates rare hairs on reproductive larvae. An = anus, Bd = bifid, Cl = clypeus, Gn = gena, Hd = head, La = labium, Lb = labrum, Ma = mandible, Mx = maxilla, PTh = prothorax, St = setae. White line indicates a scale of 100 μm.

simultaneously and continuously. As such, there may be instances where differentiating between castes, especially early in larval development, is difficult.

To further explore if our characterization of caste-specific developmental trajectories of *M. pharaonis* larvae is incomplete, we tested whether the changes in head growth we observed adhered to the Brooks–Dyar rule. This rule provides researchers with a method to statistically estimate whether they have identified the correct number of instars by evaluating whether growth between larval instars is linear and steady (Brooks 1886; Dyar 1890; O'Neal and Markin 1975). More specifically, this rule evaluates (1) whether growth between instars is linear using a linear regression model, such that when the natural logarithm (Ln) of mean head width of each instar is plotted using linear regression, the R^2 should be close to 1; and (2) whether highly sclerotized structures, in this case the larval head capsule, increases between each instar by a constant growth ratio (Crosby's ratio). Deviations > 10% in this ratio indicate that an instar may be missing, while a deviation of $> -10\%$ in this ratio indicates there may be too many annotated instars (Brooks 1886; Dyar 1890; Resh and Cardé 2009; Sukovata 2019). First, we found that the slope of mean head width of each instar is close to an $R^2 = 1$: $R^2 = 0.9983$ for worker-destined and $R^2 = 0.9954$ for reproductive-destined larvae (Supporting Information Table S1), indicating that the growth between instars is linear. Second, we found a difference that exceeds ±10% between successive growth ratios for both worker and reproductive-destined larvae (worker-destined larvae = 25.14% and reproductive-destined larvae = −12.16%). This indicates that the growth observed in our larval sample fails to adhere to the Brooks–Dyar rule. This suggests that

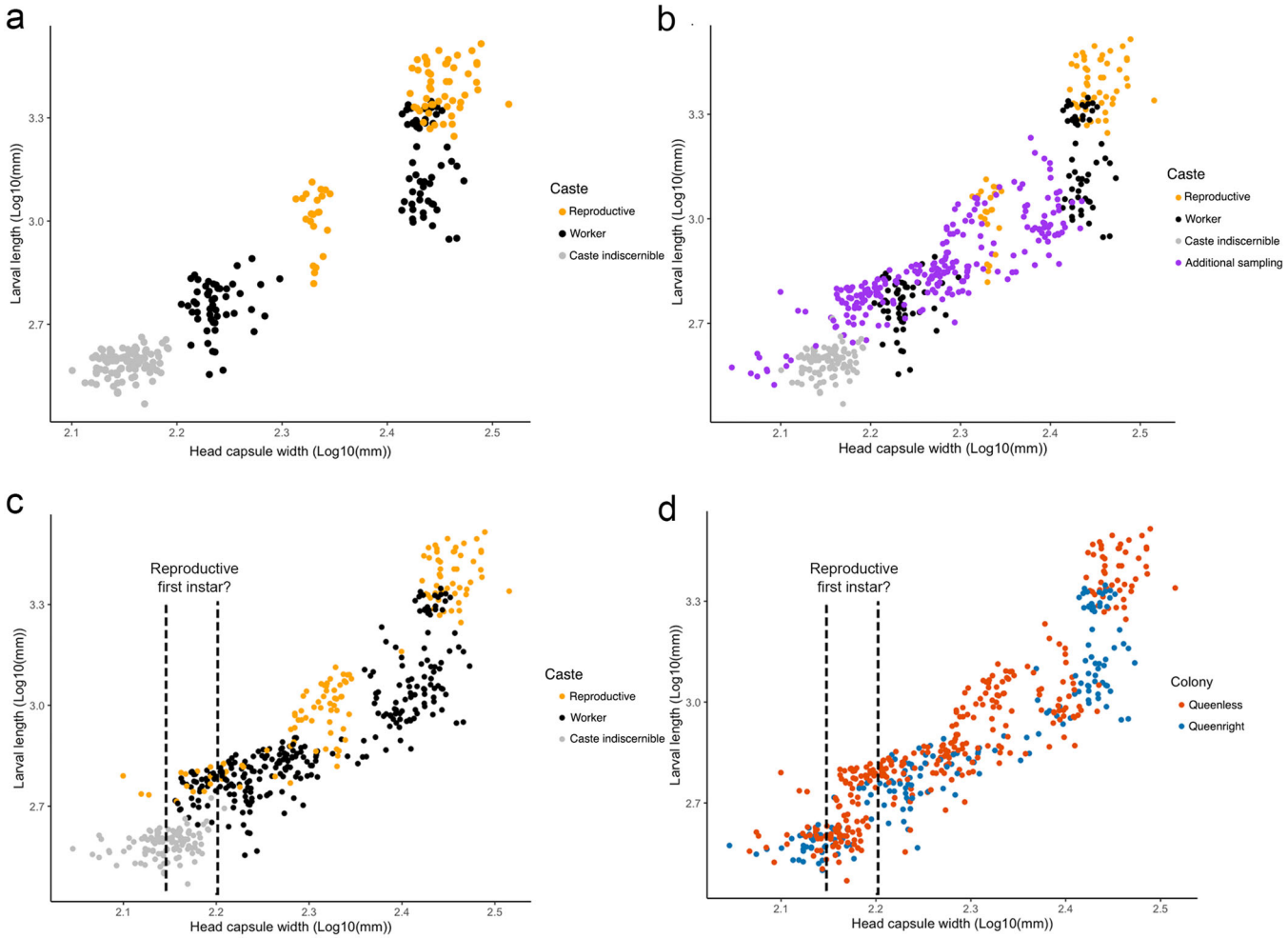

FIGURE 8 | *Monomorium pharaonis* larval instar analysis. (a) Plot of log Larval length (μm) by log Head capsule width (μm) to visualize larval instar clusters of 340 larvae, sampled according to Berndt and Eichler (1987). Gray = caste indiscernible; gold = reproductive-destined caste; black = worker-destined caste. This plot shows three instars for each caste, where the 1st instar is morphologically ambiguous. (b) Plot of log Larval length (μm) by log Head capsule width (μm) to visualize larval instar clusters with an additional 235 sampled larvae (additional Sampling; purple). (c) Plot of log Larval length (μm) by log Head capsule width (μm) of all 575 sampled larvae, annotated by caste according to their morphological landmarks. (d) Plot of log Larval length (μm) by log Head capsule width (μm) of all 575 sampled larvae, annotated by colony type they were sampled from (red = queenless; blue = queenright). Vertical dotted lines highlight the morphospace of proposed reproductive-destined 1st instar larvae.

sampling larvae based exclusively on the morphological criteria of Berndt and Eichler (1987) is insufficient to capture the full range of variation in the developmental trajectories of reproductive-destine and worker-destined larvae in *M. pharaonis*.

To address this problem, we sampled an additional 235 larvae irrespective of morphological landmarks. After measuring maximum head width and larval length of the larvae that we additionally sampled, we found that they filled the gaps in the head width morphospace between our previously annotated instar clusters (purple dots in Figure 8b). We then re-calculated Crosby's growth ratios, but this time included the additionally sampled larvae. We found that the ratio substantially improved from −12.16% to 7.99% for reproductive-destined larvae. This means that the additional sampling captured the variation previously missing in the developmental trajectories of reproductive-destined larvae because it now adheres to the Brooks-Dyar rule. However, the ratio only slightly improved from 25.14% to 20.6 percent for worker-destined larvae, suggesting two possibilities: (1) our sampling of worker-destined larvae may have erroneously included early male or gyne-destined larvae that are difficult to discern from worker-destined larvae because they are still in the process of differentiating. This would increase the variation in our worker-destined clusters (compare black dots in Figure 7a with 7c); and/or (2) other methods, such as using ecdysone titers, are needed to more precisely define the boundaries of each instar for worker-destined larvae.

Finally, our additional sampling also revealed a cluster of larvae that overlap in head capsule size with 1st instar larvae but with larger larval lengths that are similar to 2nd instar worker-destined larvae (see black and yellow dots between dotted lines in Figure 8c). Surprisingly, within this cluster is a handful of larvae that can be further annotated as reproductive-destined larvae based on morphological characters upon closer inspection (i.e., more rotund and less slender). Next, because queenless colony conditions

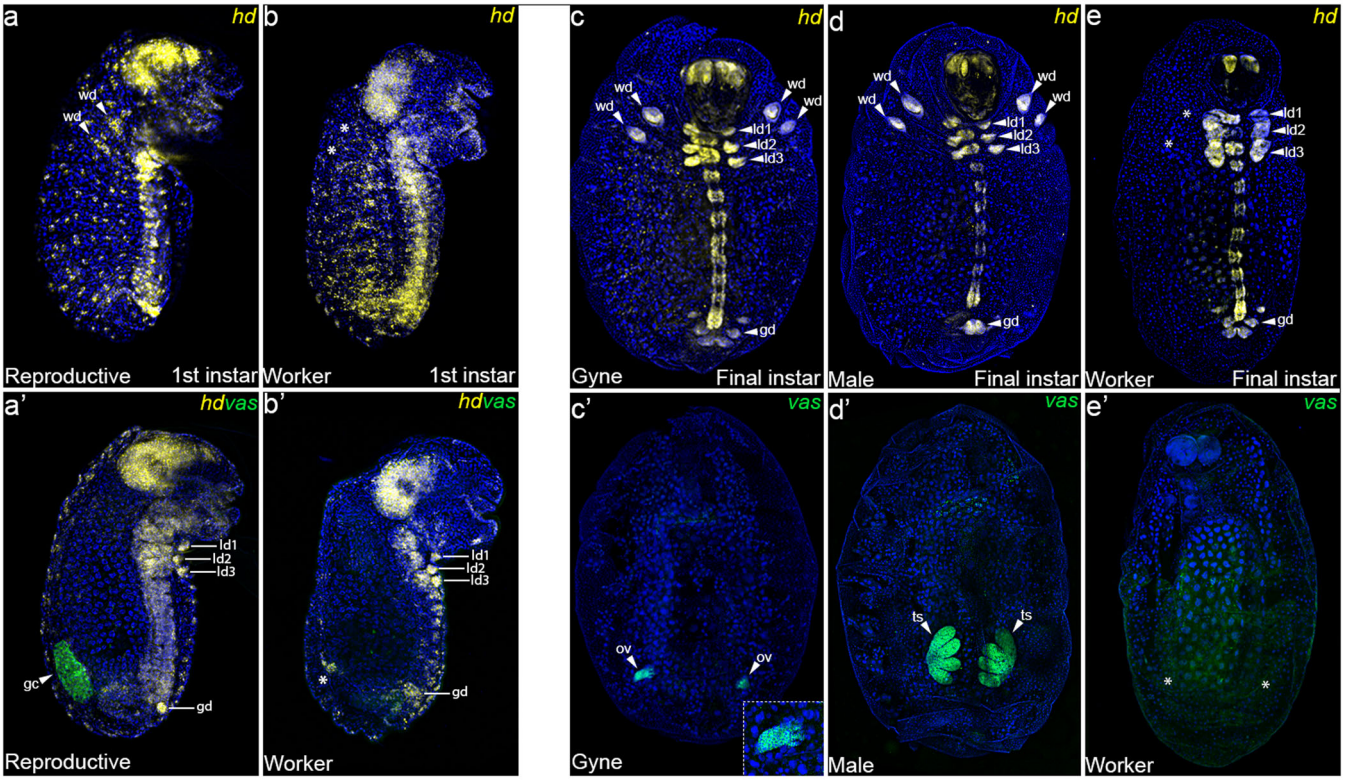

FIGURE 9 | Characterization of *Monomorium pharaonis* larval caste and sex using developmental markers. (a–e') *M. pharaonis* wholemount larvae stained with markers to distinguish caste and sex-differentiated developmental characters. (a, b) Lateral surface of a 1st instar reproductive (a) and worker (b) larvae stained with HCR probes targeting *headcase* (*hd;* yellow), an imaginal disc marker. Note, white arrows indicate the presence of wing imaginal discs (wd, a), while asterisks indicate the absence of wd (b). (a', b') Sagittal plane of a 1st instar reproductive (a') and worker (b') larvae stained with HCR probes targeting *hd*, which marks leg imaginal and genital imaginal discs (ld1-3, gd), and *vasa* (*vas*, green), which marks the larval germ cells (gc). Note, white arrow indicates the presence of germ cells (a'), while the asterisk indicates the absence of germ cells (b). (c–e) Ventral orientation of final instar gyne (c), male (d), and worker (e) larvae stained with HCR probes targeting *hd*. Note, white arrows indicate wd, ld1-3, and gd (c, d), while asterisks indicate the absence of wd (e). (c'–e') Dorsal orientation of final instar gyne (e'), male (f'), and worker (g') larvae stained with HCR probes targeting *vas*. Note, white arrows indicate the presence of ovaries (ov; c') and testes (ts; d'), while asterisks indicate the absence of ovaries (e').

increase the likelihood for reproductive-destined larvae to develop, we coded our samples based on whether larvae within the cluster came from colonies where the queen is either absent (queenless) or present (queenright) (Figure 8d). We found that almost all the larvae within this cluster came from queenless colonies (compare dotted lines in Figure 8c and d). Taken together, these results raise the possibility that within the 1st instar, putative reproductive-destined larvae accelerate their growth to establish a reproductive-specific growth trajectory. Given that we identified that reproductive and worker castes are already differentiated during early embryogenesis (Figure 5), subsequent growth within the 1st larval instar may be necessary to realize a strong queen–worker body size asymmetry during larval development.

The nearly continuous distribution in maximum head capsule size of both worker and reproductive-destined larvae coupled with their overlapping morphospace makes it difficult to establish clear instar boundaries in *M. pharaonis* (Figure 8c). This is especially evident in 2nd worker-destined larvae, where it remains difficult to define an instar boundary, as we cannot rule out that these larvae are young reproductive-destined larvae. We therefore explored whether developmental characters could further distinguish larval caste and sex (Figures 9 and 10). Previous studies have shown that final instar worker-destined larvae of *Monomorium emersoni* and *Monomorium trageri* do not develop rudiments of wing imaginal discs, while last instar gyne/queen larvae develop wing imaginal discs that develop into adult wings (Favé et al. 2015; Rajakumar et al. 2018). Moreover, it was recently shown that reproductive-destined larvae develop a germline, as marked by the expression of *vasa* mRNA, while workers do not (Qiu et al. 2022). Here, we show that 1st instar can be distinguished as reproductive or worker-destined based on the presence or absence of wing imaginal discs as marked by *headcase* expression and/or presence or absence of larval germ cells as marked by *vasa* expression (Figure 9a–b'). First instar larvae that possess wing imaginal discs and germ cells are reproductive (Figure 9a, a'), while larvae that lack wing imaginal discs and germ cells are workers (Figure 9b, b'). Similarly, probing larvae for *vasa* and *headcase* mRNA during the final larval instar can distinguish caste and sex (Figure 9c–e'). Gyne and males can be distinguished based on the morphology of the gonad marked by *vasa* (Figure 9c'–d'). Furthermore, we show that similar to other ants, morphology of the genital imaginal disc can be used to differentiate between sexes, in both live and fixed samples (Penick, Ebie, and Moore 2013) (Figure 10a–c''). As a proof-of-principle, we used the morphology of the genital disc in live larvae to annotate final instar reproductive-destined larvae as either gyne or male and found that while males and gynes have largely overlapping morphology, males are slightly smaller ($n = 51$; Figure 10d). Comparing these sex-coded samples with our previous sampling suggest that the majority of our previous sample larvae may have been gyne-destined (compare Figures 8c–10d).

Overall, the unique larval system that *M. pharaonis* (three different types of larvae simultaneously produced) allows for the rare opportunity to chart the developmental trajectories of multiple castes from the start of larval development through to metamorphosis. This knowledge can potentially provide fundamental insights into mechanisms of caste differentiation.

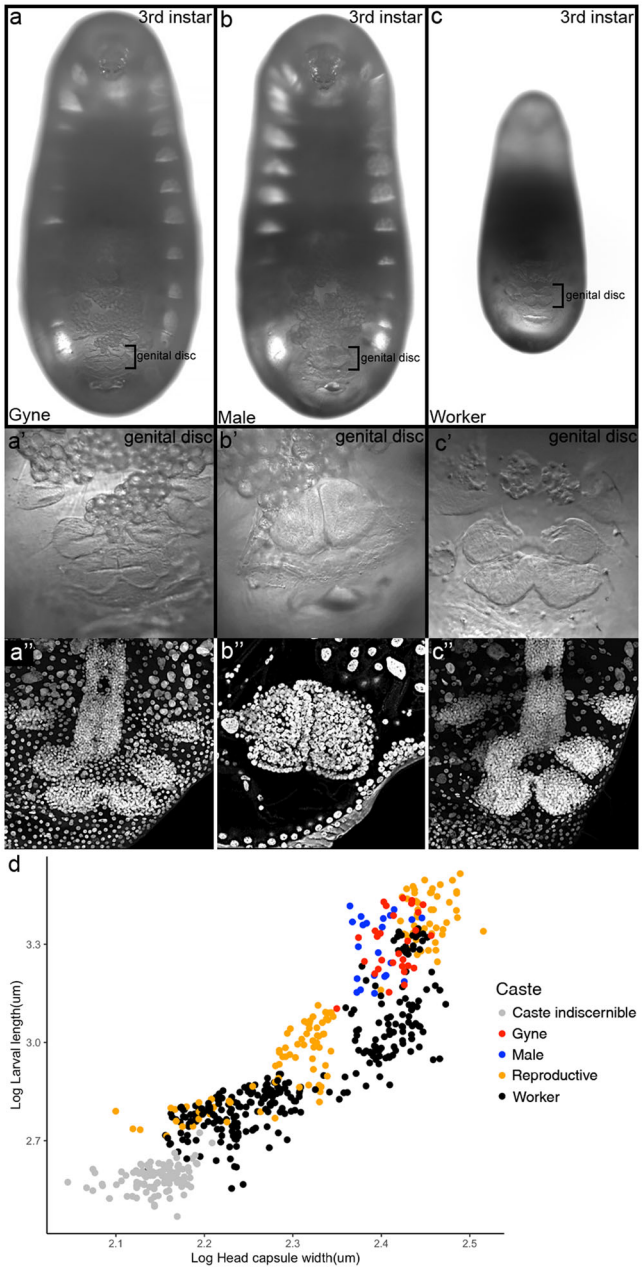

FIGURE 10 | Sexing *Monomorium pharaonis* larvae by genital disc morphology. (a–c') Brightfield images of gyne (a), male (b), and worker (c) final instar larvae. (a'–c') High magnification brightfield images of gyne (a'), male (b'), and worker (c') genital discs. Note the lotus shape of the genital disc in female castes (a', c'). (a''–c'') High magnification DAPI images of gyne (a''), male (b''), and worker (c'') genital discs. All images are to scale. Plot of log Larval length (μm) by log Head capsule width (μm) of our 575 previously sampled larvae, with an additional 66 sampled last instar reproductive-destined larvae sexed based on the morphology of their genital disc using a brightfield microscope. Gray = Caste indiscernible, gold = reproductive-destined caste, black = worker-destined caste, blue = male, red = gyne.

3.4 | Pupal Development

Pupal development for *M. pharaonis* was characterized by imaging individual workers and reproductive pupae as they aged from pupation to eclosion (Figure 11). During the prepupa stage, the size of workers (average body length ± SD: 1.576 ± 0.070; average head width ± SD: 0.269 ± 0.006, $N = 35$) is smaller than reproductives (average body length ± SD: 2.630 ± 0.103; average head width ± SD: 0.279 ± 0.010, $N = 24$). Prepupal individuals can be easily distinguished from the larval stages as the cuticle undergoes extensive wrinkling. The cuticle becomes increasingly wrinkled starting from the most posterior abdominal segments. Furthermore, prepupae are white, and the gut is colorless due to the meconium being expelled at the end of the final larval instar. Under our experimental conditions, pupal development took a total of 12 days, and there was no difference across castes in the time to eclosion. The length of pupal development varies greatly across ant lineages (Wheeler and Wheeler 1973; Lommelen, Schoeters, and Billen 2003; Ishii, Kubota, and Hara 2005), ranging from 12 to 18 days in the pavement ant *Tetramorium caespitum*, 23 days in *Cryptocerus rohweri*, and up to 36 days in the ponerine ant *Pachycondyla obscuricornis*. Whether the relatively short developmental time of *M. pharaonis* pupae may facilitate their invasive life history remains to be determined in a broader phylogenetic framework.

M. pharaonis pupae (Figure 11) are exarate and "naked" (do not spin a silk cocoon upon pupation). Worker pupae are approximately 1.5 mm long, whereas gyne and male pupae are longer (Figure 11). Pupae of all castes become increasingly darker as they age, seemingly at the same rate. Males and females can be easily distinguished from Day 1 by some morphological features. Males display bigger, ovoidal eyes, whereas the eyes of gynes are more rounded, and workers have significantly fewer ommatidia (Figure 12a–c). In males, antennae run almost parallel to the body for their entire length, whereas in females, antennae display a more pronounced angle, so that only the last antennal segments contact the body. Moreover, males and gynes possess three ocelli, a larger mesosoma, and two pairs of wings, which are

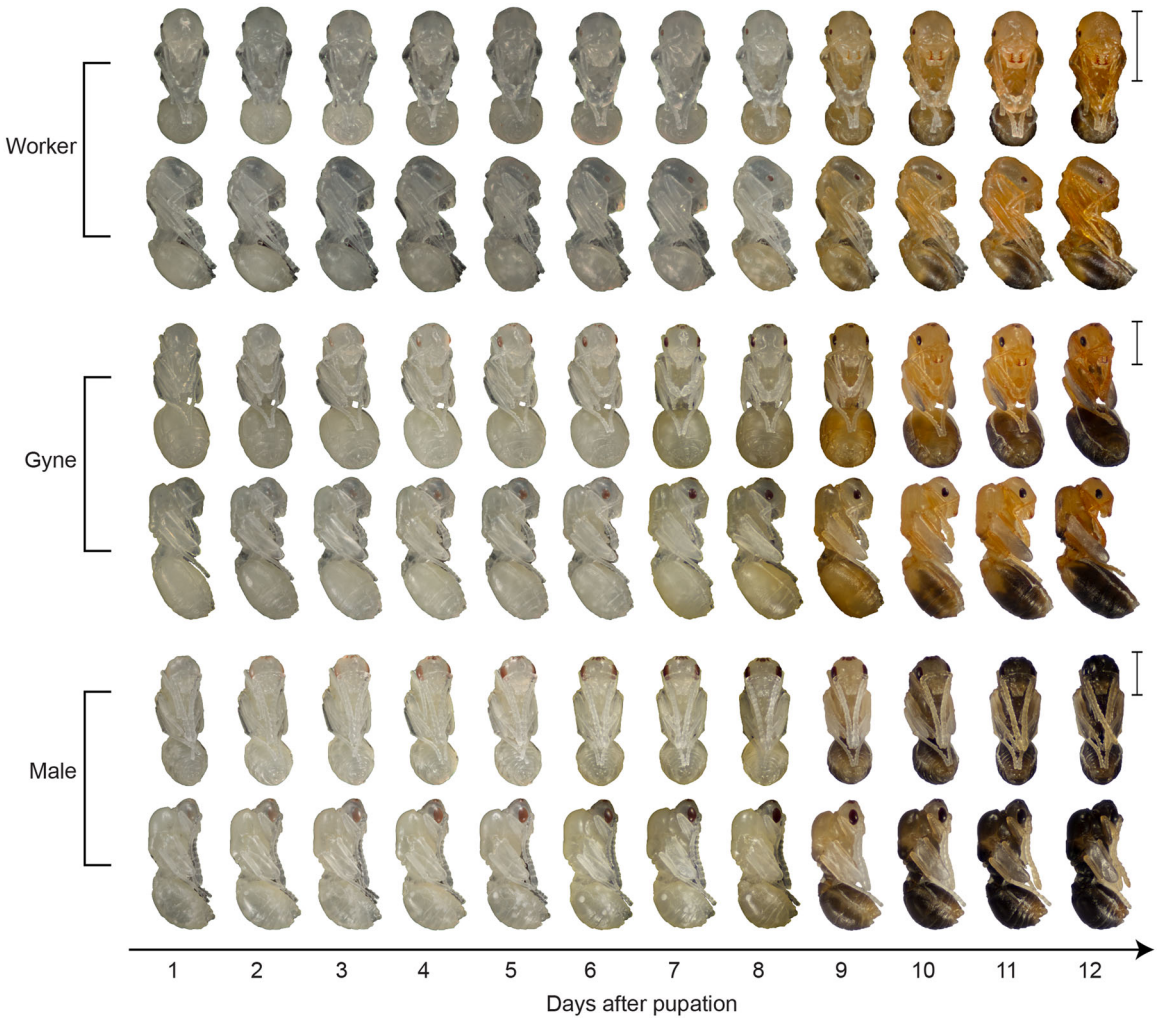

FIGURE 11 | *Monomorium pharaonis* pupal progression. Ventral (upper rows) and lateral (lower rows) views of individual worker (top), gyne (middle), and male (bottom) pupae for each day of pupal development until eclosion. Scale bar is 1 mm.

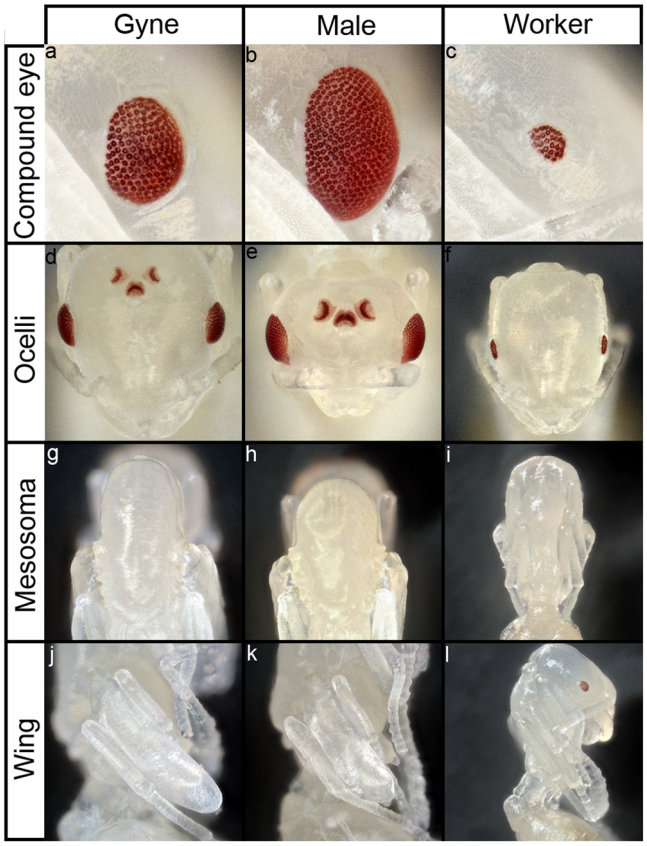

FIGURE 12 | Caste and sex-differentiated traits of *Monomorium pharaonis*. (a–l) High magnification of caste and sex-differentiated trait of gynes (left column), males (middle column), and worker (right column) pupae. (a–c) Compound eyes of gynes (a), males (b), and workers (c). Note the larger and ovoidal shape of male eyes (b) and the reduction in ommatidia in worker eyes (c). (d–f) Frontal view of the *M. pharaonis* head highlights the presence or absence of ocelli in gynes (d), males (e), and workers (f). (g–i) Dorsal view of the *M. pharaonis* thorax, highlighting size differences in mesosoma between gynes/males (g, h) and workers (I). (j–l) lateral view of the *M. pharaonis* thorax highlighting the developing wing blade in gynes (j) and males (l), while no wing blade develops in workers (l). All images across a trait are to scale.

absent in workers (Figure 12d–l). As they age, pupae acquire the characteristic coloration of the adult form: workers and gynes have an orange-brownish head and thorax, and a black abdomen (Figure 11). Males, instead, are completely black. Pigmentation begins as early as Day 2 for gyne and male pupae, and Day 3 for worker pupae. The pigmentation in all castes begins in the eyes, or eyes and ocelli for gyne and male pupae. Eye pigmentation appears to occur earlier in male than in gyne or worker pupae. Following the eyes, pigmentation proceeds in the more posterior segments of the abdomen, followed by the thorax for all castes.

Pupal development represents a hotspot for tissue morphogenesis (Gotoh et al. 2016). Therefore, the pupal stage will be of considerable interest for understanding the developmental underpinnings of the remarkable diversity in head, mandible, thorax, and petiole morphology. However, of all ontogenetic stages in ants, the pupal stage appears to be the least studied in terms of functional analysis of ant development and evolution. From a technical standpoint, the pupal stage provides some unique opportunities as the cuticle has not yet fully sclerotized and hardened. Simola et al. (2016) utilized the soft cuticle of the pupae to perform tissue-specific injections of pharmacological inhibitors to test the molecular basis of intra-caste-specific behaviors, while Miyazaki et al. (2014) injected pupae with RNAi targeting the yellow gene to understand sexually dimorphic body color. Furthermore, in *Nasonia*, *Tribolium*, and *Onthophagus*, parental RNAi is routinely performed during the pupal stage before mating to allow for the testing of maternal effects (Lynch and Desplan 2006, Lynch et al. 2011, Miller et al. 2012, Wasik and Moczek 2012, Linz et al. 2014). The largest technical hurdle for the adoption of such methodologies in ants is the ability to mate newly eclosed gynes and males in the lab for most ant systems. However, this is not an obstacle in *M. pharaonis* as adult males and gynes mate within their nests without the requirement of mating flights.

4 | Summary

We present an ant developmental staging table from egg to adult (Figure 13). Overall, development lasts approximately 45 days, with embryonic development lasting approximately 11 days, larval development approximately 22 days, and pupal development approximately 12 days. Using bright-field and DIC microscopy, we characterized the main morphogenetic events occurring over 17 stages of embryogenesis and harmonized these stages with those of *D. melanogaster* (Figure 13, green and blue shades). Using the highly conserved germline markers *nanos*, *oskar,* and Vasa, as well as live imaging, we assessed the localization of the germ cells at different developmental stages. We discovered two alternative types of germ-cell localization patterns in the embryo—the in-phenotype and the out-phenotype, which represent caste-differentiated embryos that give rise to sterile or fertile larvae and adults. Furthermore, using SEM, light microscopy, and morphometric data, we built on previous work to characterize the full range of variation of caste-specific developmental trajectories in *M. pharaonis* larvae (Alvares, Bueno, and Fowler 1993; Berndt and Eichler 1987). While we confirmed the previously described three larval instars, our analyses further revealed putative first instar reproductive-destined larvae. Moreover, using developmental and anatomical markers, we were able to differentiate larval caste and sex, which we hope will facilitate future workers on *M. pharaonis* caste differentiation. Finally, we described the pupal stages of *M. pharaonis* castes and put forward that morphogenetic mechanisms during pupal development have been largely understudied (Figure 13, orange shade). We end with the hope that this table will not only facilitate the use of *M. pharaonis* as a model for the *eco–evo–devo* of social insects but will serve as a blueprint for the generation of future developmental tables of other ant species to capture the remarkable diversity across the ants.

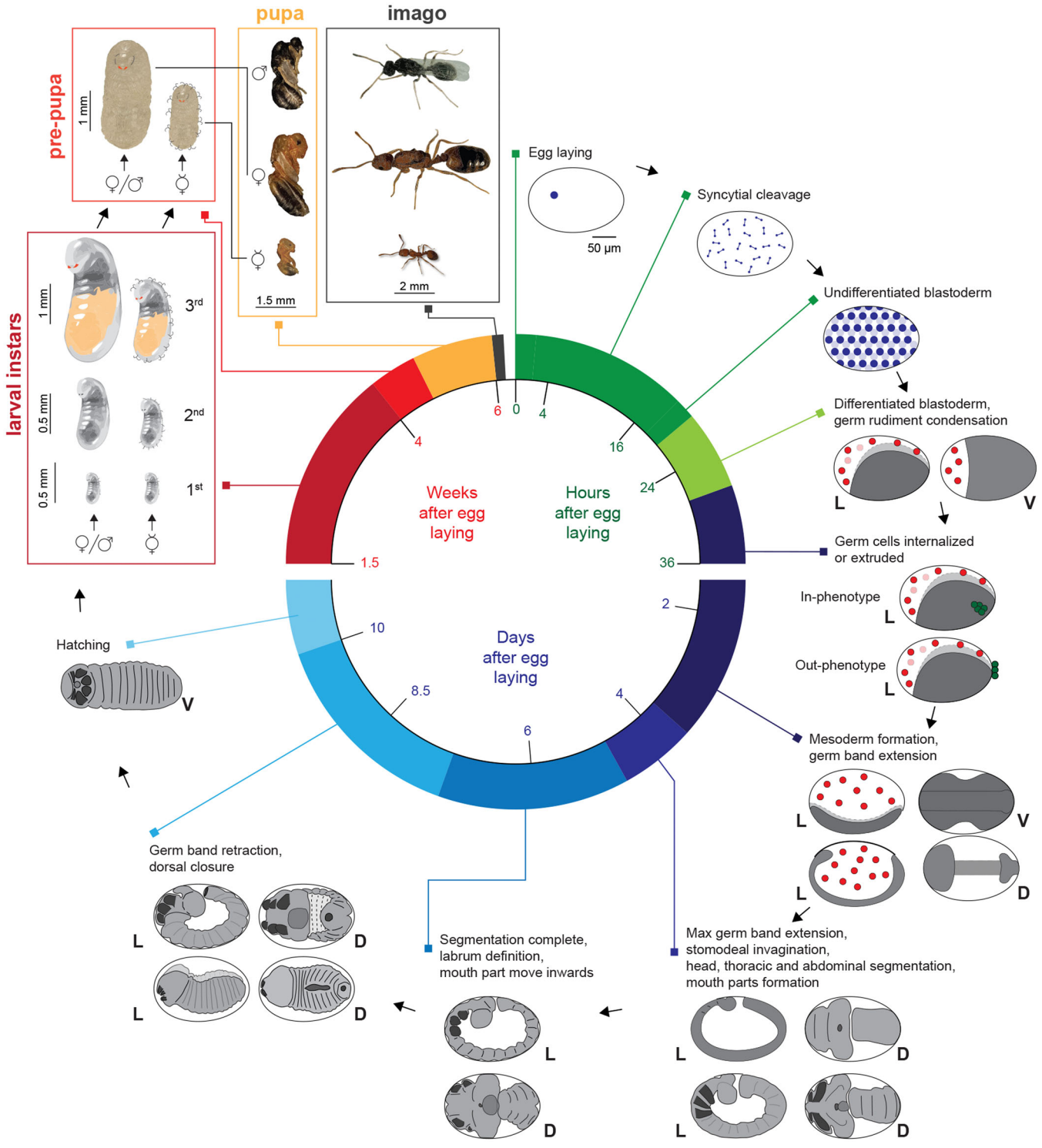

FIGURE 13 | Summary diagram of *M. pharaonis* life cycle. Green shades indicate hours after egg laying. Blue shades indicate days after egg laying. Red to Orange indicates weeks after egg laying. Gray indicates IMAGO. L = lateral, D = dorsal, V = ventral.

Author Contributions

L.P., A.R., E.A., and G.Z. conceived the project. A.R., L.P., R.S.L., G.Z., and E.A. designed experiments. A.R., L.P., R.L., R.S.L., and J.K.L.F. performed experiments. A.R., L.P., and A.M.R. matched ant embryonic descriptions to *Drosophila*. L.P., R.L., R.S.L., J.K.L.F., A.R., and A.V.-C. collected and/or analyzed larval instar data. A.R., L.P., G.Z., and E.A. wrote the manuscript.

Acknowledgments

We would like to thank the Abouheif lab for comments on the manuscript and R. Rajakumar for his advice on larval instar analyses. We would like to thank A.L. Price for her advice for troubleshooting larval HCR staining protocols. We also thank McGill University's Integrated Quantitative Biology Initiative (IQBI) and Advanced BioImaging Facility (ABIF) for imaging support. This work was supported by a doctoral fellowship from FQRNT (Québec); a Human Frontiers Science Program Long-Term Fellowship (LT0053/2022-L); and a National

Science Foundation EDGE grant (Award No. 2128304) to A.R., a Lundbeck Foundation Grant (R190-2014-2827) to G.Z., an NSERC Discovery Grant (Canada) to E.A.

Data Availability Statement

Raw data of larval instar measurements used to generate larval instar plots is provided as Supporting Information Table S1.

References

Abouheif, E., M.-J. Favé, A. S. Ibarrarán-Viniegra, M. P. Lesoway, A. M. Rafiqi, and R. Rajakumar. 2014. "Eco-Evo-Devo: The Time Has Come." In *Ecological Genomics: Ecology and the Evolution of Genes and Genomes*, edited by C. R. Landry and N. Aubin-Horth, 107–125. Dordrecht: Springer Netherlands.

Abouheif, E., and G. A. Wray. 2002. "Evolution of the Gene Network Underlying Wing Polyphenism in Ants." *Science* 297, no. 5579: 249–252.

Akam, M. 1998. "Hox Genes, Homeosis and the Evolution of Segment Identity: No Need for Hopeless Monsters." *International Journal of Developmental Biology* 42, no. 3: 445–451.

Alvarado, S., R. Rajakumar, E. Abouheif, and M. Szyf. 2015. "Epigenetic Variation in the *EGFR* Gene Generates Quantitative Variation in a Complex Trait in Ants." *Nature Communications* 6, no. 6513: 6513.

Alvares, L. E., O. C. Bueno, and H. G. Fowler. 1993. "Larval Instars and Immature Development of a Brazilian Population of Pharaoh's Ant, *Monomorium pharaonis* (L.) (Hym., Formicidae)." *Journal of Applied Entomology* 116: 90–93.

Arthur, W. 2002. "The Emerging Conceptual Framework of Evolutionary Developmental Biology." *Nature* 415: 757–764.

Athias-Henriot, C. 1947. "Recerches Sur Les Larves De Quelques Formis D'algérie." *Bulletin biologique de la France et de la Belgique* 81: 247–272.

Béhague, J., B. L. Fisher, R. Péronnet, R. Rajakumar, E. Abouheif, and M. Molet. 2018. "Lack of Interruption of the Gene Network Underlying Wing Polyphenism in an Early-Branching Ant Genus." *Journal of Experimental Zoology Part B: Molecular and Developmental Evolution* 330, no. 2: 109–117.

Bernadou, A., L. Schrader, J. Pable, E. Hoffacker, K. Meusemann, and J. Heinze. 2018. "Stress and Early Experience Underlie Dominance Status and Division of Labour in a Clonal Insect." *Proceedings of the Royal Society B: Biological Sciences* 285: 20181468.

Berndt, K.-P., and W. Eichler. 1987. "Die Pharaoameise, *Monomorium pharaonis* (L.) (Hym., Myrmicidae) Mitteilungen Aus Dem Museum Für Naturkunde in Berlin." *Zoologisches Museum und Institut für Spezielle Zoologie (Berlin)* 63: 3–186.

Bier, K. 1952. "Beziehungen Zwischen Nährzellkerngröße Und Ausbildung Ribonukleinsäurehältiger Strukturen Oocyten Von *Formica Rufa Rufo-Pratensis Minor* Gößwald." *Verhandlungen der Deutschen Zoologischen Gesellschaft in Freiburg Akademische Verlagsgesellschaft Geest & Portig K.G* 40: 369–374.

Blochmann, F. 1892. "Über Das Vorkommen Bakterienähnlicher Gebilde in Den Geweben Und Eiern Verschiedener Insekten." *Zbl Bacteriol* 11: 234–240.

Brahma, A., D. D. Frank, P. D. H. Pastor, et al. 2023. "Transcriptional and Post-Transcriptional Control of Odorant Receptor Choice in Ants." *Current Biology* 33, no. 24: 5456–5466.e5.

Brian, M. V. 1974. "Caste Differentiation in *Myrmica rubra*: The Rôle of Hormones." *Journal of Insect Physiology* 20, no. 7: 1351–1365.

Brooks, W. K. 1886. "Report on the Stomatopoda Collected by HMS Challenger During the Years 1873–76. Report on the Scientific Results of the Voyage of HMS Challenger." *Zoology* 16: 1–16. https://cir.nii.ac.jp/crid/1570572700322904832.

Bruce, H. S., and N. H. Patel. 2020. "Knockout of Crustacean Leg Patterning Genes Suggests That Insect Wings and Body Walls Evolved From Ancient Leg Segments." *Nature Ecology & Evolution* 4: 1703–1712.

Buchner, P. 1918. "Vergleichende Eistudien 1. Die Akzessorischen Kerne Des Hymenoptereneies." *Archiv für mikroskopische Anatomie* 91: 1–202.

Buchner, P. 1965. *Endosymbiosis of Animals With Plant Microorganisms*. New York: John Wiley & Sons.

Campos-Ortega, J. A., and V. Hartenstein. 1985. *The Embryonic Development of* Drosophila melanogaster. Berlin, Heidelberg: Springer.

Carroll, S. B. 1995. "Homeotic Genes and the Evolution of Arthropods and Chordates." *Nature* 376, no. 6540: 479–485.

Carroll, S. B. 2005. *Endless Forms Most Beautiful: The New Science of Evo Devo and the Making of the Animal Kingdom*. New York, USA: WW Norton & Company.

Carroll, S. B. 2008. "Evo-Devo and an Expanding Evolutionary Synthesis: A Genetic Theory of Morphological Evolution." *Cell* 134, no. 1: 25–36.

Chandra, V., I. Fetter-Pruneda, P. R. Oxley, et al. 2018. "Social Regulation of Insulin Signaling and the Evolution of Eusociality in Ants." *Science* 361, no. 6400: 398–402.

Choi, H. M. T., M. Schwarzkopf, M. E. Fornace, et al. 2018. "Third-Generation In Situ Hybridization Chain Reaction: Multiplexed, Quantitative, Sensitive, Versatile, Robust." *Development* 145, no. 12: dev165753.

Crespi, B. J., and D. Yanega. 1995. "The Definition of Eusociality." *Behavioral Ecology* 6, no. 1: 109–115.

Davidson, E. H., and D. H. Erwin. 2006. "Gene Regulatory Networks and the Evolution of Animal Body Plans." *Science* 311: 796–800. https://doi.org/10.1126/Science.1113832.

Dearden, P. K. 2006. "Germ Cell Development in the Honeybee (*Apis mellifera*); Vasa and Nanos Expression." *BMC Developmental Biology* 6, no. 6: 6. https://doi.org/10.1186/1471-213X-6-6.

Dewitz, H. 1878. "Beitrage Zur Postembryonalen Gliedmassenbildung Bei Den Insekten." *Z. Wiss. Zool.* 30: 78–105.

Dussutour, A., and S. J. Simpson. 2008. "Description of a Simple Synthetic Diet for Studying Nutritional Responses in Ants." *Insectes Sociaux* 55: 329–333. https://doi.org/10.1007/s00040-008-1008-3.

Dyar, H. G. 1890. "The Number of Molts of Lepidopterous Larvae." *Psyche: A Journal of Entomology* 5, no. 175–176: 420–422.

Ebie, J. D., B. Hölldobler, J. Liebig. 2015. "Larval Regulation of Worker Reproduction in the Polydomous ant Novomessor cockerelli." *Naturwissenschaften* 102, no. 11–12: 72.

Edwards, J. P. 1987. "Caste Regulation in the Pharaoh's Ant *Monomorium pharaonis*: The Influence of Queens on the Production of New Sexual Forms." *Physiological Entomology* 12: 31–39.

Emilia Santos, M., C. S. Berger, P. N. Refki, and A. Khila. 2015. "Integrating Evo-Devo With Ecology for a Better Understanding of Phenotypic Evolution." *Briefings in Functional Genomics* 14, no. 6: 384–395.

Evans, J. D., and D. E. Wheeler. 1999. "Differential Gene Expression Between Developing Queens and Workers in the Honey Bee, *Apis mellifera*." *Proceedings of the National Academy of Sciences of the United States of America* 96, no. 10: 5575–5580.

Extavour, C. G., and M. Akam. 2003. "Mechanisms of Germ Cell Specification Across the Metazoans: Epigenesis and Preformation." *Development* 130, no. 24: 5869–5884.

Favé, M.-J., R. A. Johnson, S. Cover, et al. 2015. "Past Climate Change on Sky Islands Drives Novelty in a Core Developmental Gene Network and Its Phenotype." *BMC Evolutionary Biology* 15, no. 183: 183.

Fleig, R., and K. Sander. 1986. "Embryogenesis of the Honeybee *Apis mellifera* L. (Hymenoptera: Apidae): An SEM Study." *International Journal of Insect Morphology and Embryology* 15: 449–462.

Fleig, R., and K. Sander. 1988. "Honeybee Morphogenesis: Embryonic Cell Movements That Shape the Larval Body." *Development* 103: 525–534.

Fox, E. G., A. A. Smith, J. C. Gibson, and D. R. Solis. 2017. "Larvae of Trap Jaw Ants, *Odontomachus* LATREILLE, 1804 (Hymenoptera: Formicidae): Morphology and Biological Notes." *Myrmecological News* 25: 17–28.

Fox, E. G., D. R. Solis, M. L. Rossi, J. H. C. Delabie, R. F. de Souza, and O. C. Bueno. 2012. "Comparative Immature Morphology of Brazilian Fire Ants (Hymenoptera: Formicidae: *Solenopsis*)." *Psyche* 2012: 10.

Ganin, M. 1869. Über die Embryonalhülle der Hymenopteren - und Lepidopteren-Embryonen Mémoires de l'Académie impériale des sciences de St. Pétersbourg 7e série 14(5).

Gerhart, J., and M. Kirschner. 1997. Cells, Embryos and Evolution: Toward a Cellular and Developmental Understanding of Phenotypic Variation and Evolutionary Adaptability. Wiley.

Gilbert, S. F., T. C. G. Bosch, and C. Ledón-Rettig. 2015. "Eco-Evo-Devo: Developmental Symbiosis and Developmental Plasticity as Evolutionary Agents." *Nature Reviews Genetics* 16: 611–622.

Glastad, K. M., L. Ju, and S. L. Berger. 2021. "Tramtrack Acts During Late Pupal Development to Direct Ant Caste Identity." *PLoS Genetics* 17, no. 9: e1009801.

Glastad, K. M., J. Roessler, J. Gospocic, R. Bonasio, and S. L. Berger. 2023. "Long Ant Life Span Is Maintained by a Unique Heat Shock Factor." *Genes & Development* 37: 398–417.

Gordon, D. M. 2019. "The Ecology of Collective Behavior in Ants." *Annual Review of Entomology* 64: 35–50. https://doi.org/10.1146/annurev-ento-011118-111923.

Gospocic, J., K. M. Glastad, L. Sheng, E. J. Shields, S. L. Berger, and R. Bonasio. 2021. "Kr-h1 Maintains Distinct Caste-Specific Neurotranscriptomes in Response to Socially Regulated Hormones." *Cell* 184, no. 23: 5807–5823.e14.

Gotoh, A., J. Billen, R. Hashim, and F. Ito. 2016. "Degeneration Patterns of the Worker Spermatheca During Morphogenesis in Ants (Hymenoptera: Formicidae)." *Evolution & Development* 18, no. 2: 96–104.

Gotoh, A., S. Sameshima, K. Tsuji, T. Matsumoto, and T. Miura. 2005. "Apoptotic Wing Degeneration and Formation of an Altruism-Regulating Glandular Appendage (Gemma) in the Ponerine Ant Diacamma Sp. From Japan (Hymenoptera, Formicidae, Ponerinae)." *Development Genes and Evolution* 215, no. 2: 69–77.

Hall, B. K. 2003. "Evo-Devo: Evolutionary Developmental Mechanisms." *International Journal of Developmental Biology* 47, no. 7–8: 491–495.

Hall, B. K. 2012. *Evolutionary Developmental Biology*. Germany: Springer Science & Business Media.

Hall, B. K., and W. M. Olson. 2006. *Keywords and Concepts in Evolutionary Developmental Biology*. Cambridge MA: Harvard University Press.

Hamilton, W. D. 1964a. "The Genetical Evolution of Social Behaviour. I." *Journal of Theoretical Biology* 7, no. 1: 1–16.

Hamilton, W. D. 1964b. "The Genetical Evolution of Social Behaviour. II." *Journal of Theoretical Biology* 7, no. 1: 17–52.

Hart, T., D. D. Frank, L. E. Lopes, et al. 2023. "Sparse and Stereotyped Encoding Implicates a Core Glomerulus for Ant Alarm Behavior." *Cell* 186, no. 14: 3079–3094.e17.

Hart, T., L. E. Lopes, D. D. Frank, and D. J. C. Kronauer. 2024. "Pheromone Representation in the Ant Antennal Lobe Changes With Age." *Current Biology* 34, no. 14: 3233–3240.e4.

Hegner, R. W. 1915. "Studies on Germ Cells. IV. Protoplasmic Differentiation in the Oocytes of Certain Hymenoptera." *Journal of Morphology* 26, no. 3: 495–561.

Hölldobler, B., and E. O. Wilson. 1990. *The Ants*. Cambridge, Massachusetts: Harvard University Press.

Hölldobler, B., and E. O. Wilson. 2009. *The Superorganism*. New York: W.W Norton & Company Inc.

Hu, Y., D. M. Linz, and A. P. Moczek. 2019. "Beetle Horns Evolved From Wing Serial Homologs." *Science* 366, no. 6488: 1004–1007.

Idogawa, N., A. Gotoh, and S. Dobata. 2022. "Morphology of Immatures of the Thelytokous Ant, *Monomorium triviale* Wheeler (Formicidae: Myrmicinae: Solenopsidini) With Descriptions of the Extraordinary Last-Instar Queen Larvae." *Zootaxa* 5105, no. 2: 253–268. https://doi.org/10.11646/ZOOTAXA.5105.2.5.

Ishii, Y., K. Kubota, and K. Hara. 2005. "Postembryonic Development of the Mushroom Bodies in the Ant, *Camponotus japonicus*." *Zoological Science* 22, no. 7: 743–753.

Jackson, D. E., M. Holcombe, and F. L. W. Ratnieks. 2004. "Trail Geometry Gives Polarity to Ant Foraging Networks." *Nature* 432: 907–909.

Ju, L., K. M. Glastad, L. Sheng, et al. 2023. "Hormonal Gatekeeping via the Blood-Brain Barrier Governs Caste-Specific Behavior in Ants." *Cell* 186, no. 20: 4289–4309.e23.

Kapheim, K. M., B. M. Jones, H. Pan, et al. 2020. "Developmental Plasticity Shapes Social Traits and Selection in a Facultatively Eusocial Bee." *Proceedings of the National Academy of Sciences of the United States of America* 117, no. 24: 13615–13625.

Khila, A., and E. Abouheif. 2008. "Reproductive Constraint Is a Developmental Mechanism That Maintains Social Harmony in Advanced Ant Societies." *Proceedings of the National Academy of Sciences of the United States of America* 105: 17884–17889.

Khila, A., and E. Abouheif. 2010. "Evaluating the Role of Reproductive Constraints in Ant Social Evolution." *Philosophical Transactions of the Royal Society B: Biological Sciences* 365: 617–630.

Klein, A., E. Schultner, H. Lowak, et al. 2016. "Evolution of Social Insect Polyphenism Facilitated by the Sex Differentiation Cascade." *PLoS Genetics* 12, no. 3: e1005952.

Koch, S., R. Tahara, A. Vasquez-Correa, and E. Abouheif. 2021. "Nano-CT Imaging of Larvae in the Ant *Pheidole Hyatti* Reveals Coordinated Growth of a Rudimentary Organ Necessary for Soldier Development." *Journal of Experimental Zoology Part B: Molecular and Developmental Evolution* 336: 540–553.

Kotadia, S., J. Crest, U. Tram, B. Riggs, and W. Sullivan. 2010. "Blastoderm Formation and Cellularisation in *Drosophila melganogaster*." *Encyclopedia of Life Sciences (ELS)*. Chichester: John Wiley & Sons. Ltd. https://doi.org/10.1002/9780470015902.a0001071.pub2.

LeBoeuf, A. C., P. Waridel, C. S. Brent, et al. 2016. "Oral Transfer of Chemical Cues, Growth Proteins and Hormones in Social Insects." *eLife* 5: e20375.

Li, Q., M. Wang, P. Zhang, et al. 2022. "A Single-Cell Transcriptomic Atlas Tracking the Neural Basis of Division of Labour in an Ant Superorganism." *Nature Ecology & Evolution* 6: 1191–1204.

Lilienstern, M. 1932. "Beiträge Zur Bakteriensymbiose Der Ameisen." *Zeitschrift Für Morphologie Und Ökologie Der Tiere* 26, no. 1/2: 110–134.

Linz, D. M., C. M. Clark-Hachtel, F. Borràs-Castells, and Y. Tomoyasu. 2014. *Journal of Visualized Experiments* 92: 52059.

Lommelen, E., E. Schoeters, and J. Billen. 2003. "Development of the Labial Gland of the Ponerine ant Pachycondyla Obscuricornis (Hymenoptera, Formicidae) During the Pupal Stage." *Arthropod Structure & Development* 32, no. 2–3: 209–217.

Londe, S., T. Monnin, R. Cornette, V. Debat, B. L. Fisher, and M. Molet. 2015. "Phenotypic Plasticity and Modularity Allow for the Production of Novel Mosaic Phenotypes in Ants." *EvoDevo* 6, no. 36: 36.

Love, A. C. 2014. "The Erotetic Organization of Developmental Biology." *Towards a Theory of Development*: 33–35. https://doi.org/10.1093/acprof:oso/9780199671427.003.0003.

Lynch, J. A., and C. Desplan. 2006. "A Method for Parental RNA Interference in the Wasp *Nasonia vitripennis*." *Nature Protocols* 1: 486–494.

Lynch, J. A., E. El-Sherif, and S. J. Brown. 2012. "Comparisons of the Embryonic Development of Drosophila, Nasonia, and Tribolium." *WIREs Developmental Biology* 1: 16–39.

Lynch, J. A., O. Özüak, A. Khila, E. Abouheif, C. Desplan, and S. Roth. 2011. "The Phylogenetic Origin of *Oskar* Coincided With the Origin of Maternally Provisioned Germ Plasm and Pole Cells at the Base of the Holometabola." *PLoS Genetics* 7, no. 4: e1002029.

Masuko, K. 2017. "Larval Instars of the Ant *Strumigenys solifontis* Brown (Hymenoptera: Formicidae): The Fallacy of Size Distribution." *Journal of Natural History* 51: 115–126.

Metzl, C., D. E. Wheeler, and E. Abouheif. 2018. "Wilhelm Goetsch (1887 - 1960): Pioneering Studies on the Development and Evolution of the Soldier Caste in Social Insects." *Myrmecological News* 26: 81–96.

Miller, S. C., K. Miyata, S. J. Brown, and Y. Tomoyasu. 2012. "Dissecting Systemic RNA Interference in the Red Flour Beetle Tribolium Castaneum: Parameters Affecting the Efficiency of RNAi." *PLoS One* 7, no. 10: e47431.

Miura, T., A. Kamikouchi, M. Sawata, et al. 1999. "Soldier Caste-Specific Gene Expression in the Mandibular Glands of *Hodotermopsis japonica* (Isoptera: Termopsidae)." *Proceedings of the National Academy of Sciences of the United States of America* 96, no. 24: 13874–13879.

Miyazaki, S., T. Murakami, T. Kubo, N. Azuma, S. Higashi, and T. Miura. 2010. "Ergatoid Queen Development in the Ant *Myrmecina nipponica*: Modular and Heterochronic Regulation of Caste Differentiation." *Proceedings of the Royal Society B: Biological Sciences* 277, no. 1690: 1953–1961.

Miyazaki, S., Y. Okada, H. Miyakawa, et al. 2014. "Sexually Dimorphic Body Color Is Regulated by Sex-Specific Expression of Yellow Gene in Ponerine Ant, Diacamma Sp." *PLoS One* 9, no. 3: e92875.

Moczek, A. P., K. E. Sears, and A. Stollewerk, et al. 2015. "The Significance and Scope of Evolutionary Developmental Biology: A Vision for the 21st Century." *Evolution & Development* 17, no. 3: 198–219.

Murugesan, S. N., H. Connahs, Y. Matsuoka, et al. 2022. "Butterfly Eyespots Evolved via Cooption of an Ancestral Gene-Regulatory Network That Also Patterns Antennae, Legs, and Wings." *Proceedings of the National Academy of Sciences of the United States of America* 119, no. 8: e2108661119.

Nagel, M., B. Qiu, L. E. Brandenborg, et al. 2020. "The Gene Expression Network Regulating Queen Brain Remodeling After Insemination and Its Parallel Use in Ants With Reproductive Workers." *Science Advances* 6, no. 38: eaaz5772. https://doi.org/10.1126/sciadv.aaz5772.

Oettler, J., T. Platschek, C. Schmidt, et al. 2019. "Interruption Points in the Wing Gene Regulatory Network Underlying Wing Polyphenism Evolved Independently in Male and Female Morphs in *Cardiocondyla* Ants." *Journal of Experimental Zoology Part B: Molecular and Developmental Evolution* 332: 7–16.

O'Neal, J., and G. P. Markin. 1975. "The Larval Instars of the Imported Fire Ant, *Solenopsis invicta* Buren (Hymenoptera: Formicidae)." *Journal of the Kansas Entomological Society* 42, no. 2: 141–151.

Panfilio, K. A. 2008. "Extraembryonic Development in Insects and the Acrobatics of Blastokinesis." *Developmental Biology* 313: 471–491.

Passera, L., and J. P. Suzzoni. 1979. "Le Role De La Reine Depheidole Pallidula (Nyl.) (Hymenoptera, Formicidae) Dans La Sexualisation Du Couvain Après Traitement Par L'hormone Juvénile." *Insectes Sociaux* 26: 343–353.

Passera, L., and C. R. Vllème. 1973. *Origine des soldats dans les sociétés de* Pheidole pallidula *(Nyl.)(Formicidae, Myrmicinae* (1973). London: Congr. IUSSI.

Patel, N. H. 1994. "Developmental Evolution: Insights From Studies of Insect Segmentation." *Science* 266, no. 5185: 581–590.

Penick, C. A., J. Ebie, and D. Moore. 2013. "A Non-Destructive Method for Identifying the Sex of Ant Larvae." *Insectes Sociaux* 61: 51–55.

Penick, C. A., S. S. Prager, and J. Liebig. 2012. "Juvenile Hormone Induces Queen Development in Late-Stage Larvae of the Ant *Harpegnathos saltator*." *Journal of Insect Physiology* 58, no. 12: 1643–1649.

Peter, I. S., and E. H. Davidson. 2016. "Implications of Developmental Gene Regulatory Networks Inside and Outside Developmental Biology." *Current Topics in Developmental Biology* 117: 237–251. https://doi.org/10.1016/Bs.Ctdb.2015.12.014.

Petralia, R. S., and S. B. Vinson. 1979. "Developmental Morphology of Larvae and Eggs of the Imported Fire Ant, *Solenopsis invicta*." *Annals of the Entomological Society of America* 72, no. 4: 472–484.

Pontieri, L., and T. A. Linksvayer. 2021. "Monomorium." *Encyclopedia of Social Insects*: 599–604. https://doi.org/10.1007/978-3-030-28102-1_171.

Pontieri, L., A. M. Schmidt, R. Singh, J. S. Pedersen, and T. A. Linksvayer. 2017. "Artificial Selection on Ant Female Caste Ratio Uncovers a Link Between Female-Biased Sex Ratios and Infection by *Wolbachia* Endosymbionts." *Journal of Evolutionary Biology* 30: 225–234.

Powell, S., S. L. Price, and D. J. C. Kronauer. 2020. "Trait Evolution Is Reversible, Repeatable, and Decoupled in the Soldier Caste of Turtle Ants." *Proceedings of the National Academy of Sciences of the United States of America* 117, no. 12: 6608–6615.

Qiu, B., X. Dai, P. Li, et al. 2022. "Canalized Gene Expression During Development Mediates Caste Differentiation in Ants." *Nature Ecology & Evolution* 6: 1753–1765. https://doi.org/10.1038/s41559-022-01884-y.

Qui, B., R. Stenbak Larsen, N.-C. Chang, J. Wang, J. J. Boomsma, and G. Zhang. 2018. "Towards Reconstructing the Ancestral Brain Gene-Network Regulating Caste Differentiation in Ants." *Nature Ecology & Evolution* 2: 1782–1791.

Quiring, R., U. Walldorf, U. Kloter, and W. J. Gehring. 1994. "Homology of the Eyeless Gene of *Drosophila* to the Small Eye Gene in Mice and Aniridia in Humans." *Science* 265, no. 5173: 785–789.

Rafiqi, A. M., S. Lemke, S. Ferguson, M. Stauber, and U. Schmidt-Ott. 2008. "Evolutionary Origin of the Amnioserosa in Cyclorrhaphan Flies Correlates With Spatial and Temporal Expression Changes of *Zen*." *Proceedings of the National Academy of Sciences of the United States of America* 105, no. 1: 234–239.

Rafiqi, A. M., S. Lemke, and U. Schmidt-Ott. 2011. "*Megaselia abdita*: Fixing and Devitelinizing Embryos." *Cold Spring Harbor Protocol*: 4aac29-431. https://doi.org/10.1101/pdb.prot5602.

Rafiqi, A. M., A. Rajakumar, and E. Abouheif. 2020. "Origin and Elaboration of a Major Evolutionary Transition in Individuality." *Nature* 585: 239–244.

Rajakumar, R., S. Koch, M. Couture, et al. 2018. "Social Regulation of a Rudimentary Organ Generates Complex Worker-Caste Systems in Ants." *Nature* 562: 574–577.

Rajakumar, R., D. San Mauro, M. B. Dijkstra, et al. 2012. "Ancestral Developmental Potential Facilitates Parallel Evolution in Ants." *Science* 335, no. 6064: 79–82.

Resh, V., and R. T. Cardé. 2009. *Encyclopedia of Insects*. 2nd ed., 432–433. San Diego CA: Academic Press.

Rueden, C. T., J. Schindelin, M. C. Hiner, et al. 2017. "ImageJ2: Imagej for the Next Generation of Scientific Image Data." *BMC Bioinformatics* 18: 529.

Sameshima, S.-Y., T. Miura, and T. Matsumoto. 2004. "Wing Disc Development During Caste Differentiation in the Ant *Pheidole megacephala* (Hymenoptera: Formicidae)." *Evolution & Development* 6, no. 5: 336–341.

Sanger, T. J., and R. Rajakumar. 2018. "How a Growing Organismal Perspective Is Adding New Depth to Integrative Studies of Morphological Evolution." *Biological Reviews* 94: 184–198.

Schmidt, A. M., T. A. Linksvayer, J. J. Boomsma, and J. S. Pedersen. 2010. "Queen–Worker Caste Ratio Depends on Colony Size in the Pharaoh ant *Monomorium pharaonis*." *Insectes Sociaux* 58, no. 2: 139–144. https://doi.org/10.1007/s00040-010-0126-x.

Schmidt, A. M., T. A. Linksvayer, J. J. Boomsma, and J. S. Pedersen. 2011. "No Benefit in Diversity? The Effect of Genetic Variation on Survival and Disease Resistance in a Polygynous Social Insect." *Ecological Entomology* 36, no. 6: 751–759.

Schrader, L., J. W. Kim, D. Ence, et al. 2014. "Transposable Element Islands Facilitate Adaptation to Novel Environments in an Invasive Species." *Nature Communications* 5, no. 5495: 5495. https://doi.org/10.1038/ncomms6495.

Schrader, L., M. Winter, M. Errbii, J. Delabie, J. Oettler, and J. Gadau. 2021. "Inhibition of HSP90 Causes Morphological Variation in the Invasive Ant *Cardiocondyla obscurior*." *Journal of Experimental Zoology Part B: Molecular and Developmental Evolution* 336, no. 4: 333–340.

Schultner, E., J. Oettler, and H. Helanterä. 2017. "The Role of Brood in Eusocial Hymenoptera." *Quarterly Review of Biology* 92: 39–78.

Simola, D. F., R. J. Graham, C. M. Brady, et al. 2016. "Epigenetic (Re) Programming of Caste-Specific Behavior in the Ant *Camponotus floridanus*." *Science* 351, no. 6268: aac6633.

Singh, R., and T. A. Linksvayer. 2020. "*Wolbachia*-Infected Ant Colonies Have Increased Reproductive Investment and an Accelerated Life Cycle." *Journal of Experimental Biology* 223: jeb220079.

Snir, O., H. Alwaseem, S. Heissel, et al. 2022. "The Pupal Moulting Fluid Has Evolved Social Functions in Ants." *Nature* 612: 488–494.

Solis, D. R., E. G. P. Fox, L. M. Kato, et al. 2010. "Morphological Description of the Immatures of the Ant, *Monomorium floricola*." *Journal of Insect Science* 10, no. 1: 15

Sommer, R. J., and M. G. Mayer. 2015. "Toward a Synthesis of Developmental Biology With Evolutionary Theory and Ecology." *Annual Review of Cell and Developmental Biology* 31, no. 1: 453–471.

Stathopoulos, A., and S. Newcomb. 2020. "Setting up for Gastrulation: *D. melanogaster*." *Current Topics in Developmental Biology* 136: 3–32.

Strindberg, H. 1913. Einige Stadien der Embryonalentwicklung bei Myrmica rubra unter besonderer Berücksichtigung der sogenannten Entodermfrage 41: 512–521.

Strindberg, H. 1915a. "Zur Eifurchung der Hymenopteren nebst einigen damit zusammenhängenden Fragen." *Zoologischer Anzeiger* 45: 248–260.

Strindberg, H. 1915b. "Noch Eine Ameise Ohne Serosa (*Tetramorium Caespitum* L.)." *Zoologischer Anzeiger* 46: 198–202.

Strindberg, H. 1916. "Neue Studien Über Ameisenembryologie." *Zoologischer Anzeiger* 7: 178–197.

Strindberg, H. 1917. "Oie Eifurchung Von *Tapinoma Erraticum* Latr." *Zoologischer Anzeiger* 50: 204–207.

Sukovata, L. 2019. "A Comparison of Three Approaches for Larval Instar Separation in Insects – A Case Study of *Dendrolimus pini*." *Insects* 10, no. 11: 384.

Tanquary, M. C. 1912. *Biological and Embryological Studies on Formicidae*. PhD thesis, University of Illinois.

Teseo, S., N. Châline, P. Jaisson, and D. J. C. Kronauer. 2014. "Epistasis Between Adults and Larvae Underlies Caste Fate and Fitness in a Clonal Ant." *Nature Communications* 5: 3363.

Toth, A. L., and S. M. Rehan. 2017. "Molecular Evolution of Insect Sociality: An Eco-Evo-Devo Perspective." *Annual Review of Entomology* 62: 419–442.

Trible, W., V. Chandra, K. D. Lacy, et al. 2023. "A Caste Differentiation Mutant Elucidates the Evolution of Socially Parasitic Ants." *Current Biology* 33, no. 6: 1047–1058.e4.

Trible, W., L. Olivos-Cisneros, S. K. McKenzie, et al. 2017. "*orco* Mutagenesis Causes Loss of Antennal Lobe Glomeruli and Impaired Social Behavior in Ants." *Cell* 170: 727–735.e10.

Villalta, I., E. Angulo, S. Devers, X. Cerdá, and R. Boulay. 2015. "Regulation of Worker Egg Laying by Larvae in a Fission-Performing ant." *Animal Behaviour* 106: 149–156.

Wagner, G. 2014. *Homology, Genes, and Evolutionary Innovation*. Princeton, Oxford: Princeton University Press.

Walsh, J. T., S. Garnier, and T. A. Linksvayer. 2020. "Ant Collective Behaviour Is Heritable and Shaped by Selection." *American Naturalist* 196, no. 5: 541–554.

Walsh, J. T., M. R. Warner, A. Kase, B. J. Cushing, and T. A. Linksvayer. 2018. "Ant Nurse Workers Exhibit Behavioural and Transcriptomic Signatures of Specialization on Larval Stage." *Animal Behaviour* 141: 161–169.

Warner, M. R., K. Kovaka, and T. A. Linksvayer. 2016. "Late-Instar Ant Worker Larvae Play a Prominent Role in Colony-Level Caste Regulation." *Insectes Sociaux* 63: 575–583.

Warner, M. R., J. Lipponen, and T. A. Linksvayer. 2018. "Pharaoh Ant Colonies Dynamically Regulate Reproductive Allocation Based on Colony Demography." *Behavioral Ecology and Sociobiology* 72, no. 3: 31.

Warner, M. R., A. S. Mikheyev, and T. A. Linksvayer. 2019. "Transcriptomic Basis and Evolution of the Ant Nurse-Larval Social Interactome." *PLoS Genetics* 15: e1008156.

Warner, M. R., L. Qui, M. J. Holmes, A. S. Mikheyev, and T. Linksvayer. 2019. "Covergent Eusocial Evolution Is Based on a Shared Reproductive Groundplan Plus Lineage-Specific Plastic Genes." *Nature Communications* 10, no. 2651. https://doi.org/10.1038/s41467-019-10546-w.

Wasik, B. R., and A. P. Moczek. 2012. "*pangolin* Expression Influences the Development of a Morphological Novelty: Beetle Horns." *Genesis* 50: 404–414.

West-Eberhard, M. J. 2003. *Developmental Plasticity and Evolution*. Oxford, New York: Oxford University Press.

Wheeler, D. E. 1982. "Soldier Determination in the Ant Pheidole bicarinata." PhD diss., Duke University.

Wheeler, D. E. 1986. "Developmental and Physiological Determinants of Caste in Social Hymenoptera – Evolutionary Implications." *American Naturalist* 128, no. 1: 13–34.

Wheeler, D. E., and H. F. Nijhout. 1981a. "Imaginal Wing Discs in Larvae of the Soldier Caste of *Pheidole bicarinata vinelandica*

Florel (Hymenoptera: Formicidae)." *International Journal of Insect Morphology and Embryology* 10,no.2: 131–139.

Wheeler, D. E., and H. F. Nijhout. 1981b. "Soldier Determination in Ants: New Role for Juvenile Hormone." *Science* 213, no. 4505: 361–363.

Wheerler, D. E., and H. F. Nijhout. 2003. "Soldier Determination in *Pheidole bicarinata*: Effect of Methoprene on Caste and Size Within Castes." *Journal of Insect Physiology* 29, no. 11: 847–854.

Wheeler, G. C., and J. Wheeler. 1953. "The Ant Larvae of the Subfamily Formicinae." *Annals of the Entomological Society of America* 46: 126–171. https://doi.org/10.1093/aesa/46.1.126.

Wheeler, G. C., and J. Wheeler. 1955. "The Ant Larvae of the Myrmicine Tribe Solenopsidini." *American Midland Naturalist* 54: 119–141. https://doi.org/10.2307/2422182.

Wheeler, G. C., and J. Wheeler. 1973. "Ant Larvae of Four Tribes: Second Supplement (Hymenoptera: Formicidae: Myrmicinae)." *Psyche: A Journal of Entomology* 80, no. 1–2: 70–82.

Wheeler, G. C., and J. Wheeler. 1976. *Ant Larvae: Review and Synthesis*. Vol. 7. Washington, DC: Entomological Society of Washington.

Wheeler, G. C., and J. Wheeler. 1990. Notes on Ant Larvae Transactions of the American Entomological Society 115: 457–473.

Wheeler, W. M. 1893. "A Contribution to Insect Embryology." *Journal of Morphology* 8, no. 1: 1–161.

Wheeler, W. M. 1910. *Ants: Their Structure, Development and Behavior*. New York: The Columbia University Press.

Wheeler, W. M. 1911. "The Ant-Colony as an Organism." *Journal of Morphology* 22: 307–325.

Wheeler, W. M. 1918. "A Study of Some Ant Larvae, With a Consideration of the Origin and Meaning of the Social Habit Among Insects." *Proceedings of the American Philosophical Society* 57, no. 4: 293–343.

Wheeler, W. M. 1922. "II. The Ants Collected by the American Museum Congo Expedition." *Bulletin of the American Museum of Natural History* 45: 39–269.

Wilson, E. O. 1954. "A New Interpretation of the Frequency Curves Associated With Ant Polymorphism." *Insectes Sociaux* 1: 75–80.

Yan, H., C. Opachaloemphan, F. Carmona-Aldana, et al. 2022. "Insulin Signaling in the Long-Lived Reproductive Caste of Ants." *Science* 377, no. 6610: 1092–1099.

Yan, H., C. Opachaloemphan, G. Mancini, et al. 2017. "An Engineered *Orco* Mutation Produces Aberrant Social Behavior and Defective Neural Development in Ants." *Cell* 170: 736–747.e9.

Yang, A. S., and E. Abouheif. 2011. "Gynandromorphs as Indicators of Modularity and Evolvability in Ants." *Journal of Experimental Zoology Part B: Molecular and Developmental Evolution* 316B, no. 5: 313–318.

Supporting Information

Additional supporting information can be found online in the Supporting Information section.